

MATRIX METHOD OF SOLUTION FOR
COUPLED BOLTZMANN EQUATIONS AND ITS
APPLICATIONS TO SUPERFLUID
 ^3He AND SEMICONDUCTORS

By

YUANSHAN SUN

A DISSERTATION PRESENTED
TO THE GRADUATE SCHOOL
OF THE UNIVERSITY OF FLORIDA IN
PARTIAL FULFILLMENT OF THE REQUIREMENTS
FOR THE DEGREE OF DOCTOR OF PHILOSOPHY

UNIVERSITY OF FLORIDA

1990

To My Parents

ACKNOWLEDGEMENTS

I am extremely grateful to my advisor Professor Peter K. Wölflé from whom I have learnt so much in the past few years. His collaboration, encouragement, patience and timely advice have been invaluable throughout the course of my research.

I am very grateful to Dr. Christopher J. Stanton for his encouragement and guidance in my research in femtosecond relaxation processes in semiconductors.

I wish to thank Professors James W. Dufty, Neil S. Sullivan, Myron N. Chang for serving on my supervisory committee. I wish to thank Dr. Peter Hirschfeld for his very helpful suggestions and discussions. I am grateful to Professor T. Li and Dr. Yip whose lively discussions and collaboration provided a strong impetus to my research. I wish to thank all the other people from whom I have learnt physics: the faculty members of the physics department, particularly those in the condensed matter theory group.

It is a pleasure to thank my fellow graduate students Johann Kroha, Stephan Schiller, Chang Sub Kim, David Kilcrease, Laddawan Ruamsuwan for their help with the computer work and useful discussions.

This research was supported in part by the National Science Foundation grants DMR-8607941 and by the Institute for Fundamental Theory.

TABLE OF CONTENTS

	<i>page</i>
ACKNOWLEDGEMENTS	iii
ABSTRACT	vi
CHAPTERS	
1 INTRODUCTION	1
2 THERMAL TRANSPORT IN SUPERFLUID ^3He	9
2.1 Two Fluid Model	9
2.2 Kinetic equations	14
2.3 Solution for Half Space Case	16
2.4 Solution for Sandwich Case	21
3 HYDRODYNAMIC LIMIT	25
3.1 Hydrodynamic Description	25
3.2 Hydrodynamic Limit Approach	29
3.3 Thermal Decay Length	31
4 NUMERICAL SOLUTIONS	33
4.1 Half Space Case	33
4.2 Sandwich Case	35
5 MACROSCOPIC BOUNDARY CONDITION	46
5.1 Entropy Flow and Superfluid Flow	46
5.2 Onsager Coefficients	48
5.3 Slip Length	55
6 BOUNDARY THERMAL RESISTANCE	59
6.1 Hydrodynamic Regime	59

6.2 Knudsen Regime	62
6.3 Results from Onsager Coefficients	63
7 DISCUSSION OF ^4He CASE	68
7.1 Kinetic Equation for ^4He in Phonon Case	68
7.2 Bounds for the Ratio $v_n(\infty)/\delta T_L$	70
8 FEMTOSECOND RELAXATION IN BULK GaAs	76
8.1 Band Structure	76
8.2 Scattering Mechanisms	77
8.3 Detailed Balance	81
9 SOLUTION OF BOLTZMANN EQUATIONS	83
9.1 Coupled Boltzmann Equations	83
9.2 Matrix Method Solution	85
10 RELAXATION PROCESSES	88
10.1 Numerical Results	88
10.2 Nonparabolicity	90
11 SUMMARY AND DISCUSSION	101
APPENDICES	
A LANDAU-BOLTZMANN EQUATION	107
B ONSAGER RELATION	109
C BOUNDARY CONDITION FOR $\delta f_p^{\mu(+)}$	111
REFERENCES	115
BIOGRAPHICAL SKETCH	121

Abstract of Dissertation Presented to the Graduate School
of the University of Florida in Partial Fulfillment of the
Requirements for the Degree of Doctor of Philosophy

MATRIX METHOD OF SOLUTION FOR
COUPLED BOLTZMANN EQUATIONS AND ITS
APPLICATIONS TO SUPERFLUID
 ^3He AND SEMICONDUCTORS

By

Yuanshan Sun

May 1990

Chairman: Peter K. Wölfle
Major Department: Physics

A matrix method of solution for a set of coupled Boltzmann equations and its applications to the thermal transport across boundaries in superfluid ^3He and the femtosecond relaxation of laser-excited electrons in GaAs are presented in this dissertation. In the first part, the temperature and normal fluid velocity of superfluid ^3He between parallel plates have been calculated in the presence of a stationary heat flow normal to the plates. The system is modelled by Landau-Boltzmann equation and a diffuse scattering mechanism at the boundaries. In the hydrodynamic regime the temperature jump at the wall turns out to be small, but is replaced by a large amplitude exponential regime of macroscopic characteristic length. The three Onsager coefficients proposed recently by Grabinski and Liu are determined. In the Knudsen regime the thermal boundary resistance is found to increase exponentially with decreasing temperature. The case of ^4He is briefly discussed.

In the second part, the transient distribution functions of laser-excited electrons in the Γ and L valleys are presented by solving a set of coupled rate equations resulting from the coarse graining of the Boltzmann equation. The

distribution functions obtained from this new method agree extremely well with those obtained from the more computationally intensive Monte Carlo approach. On a longer time scale, oscillations occur in the distribution functions and agree with those obtained from hot luminescence spectrum. The separation in energy between the peaks of the electron distribution in the conduction band clearly shows the role of polar optic phonon scattering in the relaxation processes. Our results also show that a shoulder-like feature in the luminescence spectrum above 0.3eV is not due to the emission of an 8meV TA phonon as originally suggested.

CHAPTER 1 INTRODUCTION

The Boltzmann equation deals with physical kinetics in the wide sense of the microscopic theory of processes in nonequilibrium system.^{1,2} Even though the Monte Carlo approach has been emphasized recently in solving the integro-differential Boltzmann equations because of the difficulty and limitation of exact analytical solutions,³ it is still worthwhile to explore the analytical methods of solution both for physical and mathematical considerations.^{4,5,6} A matrix method of solution for a set of coupled Boltzmann equations and its applications to the thermal transport across boundaries in superfluid ^3He and the femtosecond relaxation of laser-excited electrons in GaAs are presented in this dissertation, which is organized as follows, in essentially two parts. In the first part related to the superfluid ^3He , we consider a stationary process. This process involves normal flow and superfluid counter flow and is therefore a coupled mass flow and heat flow problem.

There has been considerable interest recently in the flow of quantum liquids in restricted geometries.⁷ For one, the interpretation of flow experiments in terms of bulk properties of the liquid requires knowledge of the effect of the boundaries. Secondly, the nature of the interaction of a quantum liquid with a solid surface is an interesting problem in its own right, which is still largely unexplored. One may distinguish two different situations, depending on whether the influence of the interaction of the particles in the liquid with the boundary disturb the thermodynamic equilibrium state of the liquid over a short or long

range. For flow channels of extension large as compared to the mean free path ℓ of thermal excitations a hydrodynamic description supplemented by appropriate macroscopic boundary conditions is adequate. In the opposite limit, the so-called Knudsen regime, a microscopic description in terms of a distribution function for thermal excitations becomes necessary.

In experiments on liquid ^3He investigating the stationary Poiseuille flow through capillaries,⁸ the damping of torsional oscillators^{9,10} and vibrating wires immersed in the fluid,¹¹ and the propagation of fourth^{12,13} and first^{14,15} sound, it has been found that a pure hydrodynamic description becomes inadequate at low temperatures, when the mean free path of the thermal excitations becomes comparable to the characteristic dimensions of the experiment. Under these circumstances the interaction of the thermal excitations with the walls of the container must be taken into account more rigorously than by imposing a simple hydrodynamic boundary condition, for example, requiring the fluid to stick to the wall. In the regime of small deviations from hydrodynamics, one may relax the sticking condition to allow for fluid slip, characterized by a characteristic length, the slip length, defined as the velocity of the fluid at the wall to its spatial derivative,¹⁶ when the mean free path of thermal excitations is comparable to, or even larger than the dimensions of the container, hydrodynamic theory has to be abandoned. In this case a full kinetic description in terms of a distribution function for quasiparticles in momentum space is inevitable.

While transverse flow has been studied extensively, including the effect of different types of interaction of the thermal excitations with the channel walls for both normal and superfluid quantum liquids,^{17–21} both the slip length and

the complete distribution functions have been calculated in a transverse flow situation.^{18,19}

Flow in the form of thermal counterflow in a superfluid has not yet attracted similar attention. In this work, for the first time, the macroscopic boundary conditions and the thermal boundary resistance in the hydrodynamic regime, as well as the thermal counter flow in the Knudsen regime for the diffuse scattering model of a surface have been calculated.

If we assume the boundary to be impenetrable for quasiparticles, the mass flow of the quasiparticles has to be balanced by a superflow in the opposite direction, such that the total mass flow is zero. Thus we address the question of boundary effects on normal counterflow. This counterflow problem, since the normal component carries the entropy and hence the heat flux, is automatically a coupled heat and mass flow problem. In general a temperature gradient will be set up.

It was shown recently by Grabinski and Liu^{22,23} that even in the hydrodynamic regime the macroscopic boundary conditions for the case of thermal flow are more complex than previously thought. In particular, they found that the boundary conditions suggested by Khalatnikov²⁴ are not general enough when dissipation is taken into account. The general hydrodynamic boundary conditions derived by Grabinski and Liu²² relate the entropy flow f_0 and the superfluid mass flow j_s (in the rest frame of the normal fluid) at the boundary to the temperature jump ΔT and the normal fluid velocity gradient (dv_n/dx) as

$$f_0 = a\Delta T + c(\alpha v'_n + \beta g^l)/\rho \quad (1.1)$$

$$j_s = c\Delta T + b(\alpha v'_n + \beta g^l)/\rho \quad (1.2)$$

Here we are considering, for definiteness, a wall on the left and the superfluid on the right of the surface at which the above equations should be applied. ΔT is the temperature jump at the boundary, v_n is the normal fluid velocity, g is the number current density in the laboratory frame, ρ is the number density, f_o is the entropy flux density in the rest frame of the wall, j_s is the superfluid number density in the normal fluid rest frame, α, β are combinations of shear viscosity η and second viscosities $\zeta_{1,2,3}$:²⁵ $\alpha = \frac{4}{3}\eta - 2\zeta_1\rho + \zeta_2 + \zeta_3\rho^2$, and $\beta = \zeta_1 - \zeta_3\rho$, a, b, c are surface Onsager coefficients, with $a, b > 0$ and $ab \geq c^2$. The hydrodynamic formula for the various fluxes are

$$f_0 = -\frac{s}{\rho}j_s - \kappa\frac{\nabla T}{T} \quad (1.3)$$

$$j_s = \rho_s(v_s - v_n) \quad (1.4)$$

here s is the entropy density, κ is the thermal conductivity, ρ_s is the superfluid number density, and the velocities are with respect to the laboratory frame.

The derivation of eqs.(1.1) to (1.4) from microscopic theory is an open problem. Given the temperature of the wall or the entropy flow f , one would like to calculate the magnitude of the three Onsager coefficients, the temperature jump at the wall, the normal velocity profile, the thermal boundary resistance and so on. It requires in principle a microscopic description of the interaction of the quasiparticles of the superfluid with the boundary. At present a microscopic theory on the atomic scale is not feasible. However, we expect simple models of the surface such as the diffuse scattering model or the specular scattering model to account for the qualitative effects of the surface. In the superfluid state, the interaction of Bogoliubov quasiparticles with a surface may be strongly affected by the possible distortions of the gap parameter

near the surface^{26,27} and also Andreev reflections will occur near the wall.^{26,28} These effects will be neglected here for simplicity.

The kinetic equation of the Bogoliubov quasiparticles is presented first in this part of the dissertation. By using conservation laws and introducing the chemical potential μ_n of the quasiparticles as a quasihydrodynamic variable, we obtain a set of coupled integro-differential equations related to the temperature, normal fluid velocity and chemical potential both for the sandwich case (parallel plate geometry) and the half space case (half infinite geometry).

Secondly, a hydrodynamic limit approach to the coupled equations is calculated, and is verified to coincide with the previous hydrodynamic description by entropy, thermal conductivity and viscosities. The thermal decay length λ as function of energy gap $\Delta/k_B T$ has been obtained and this is very beneficial in the numerical calculation for the half space case and also in the comparison of the microscopic results with the hydrodynamic descriptions.

Thirdly, the numerical solutions of the coupled integro-differential equations are obtained for an isotropic Fermi superfluid. By fitting the numerical results for a slab of width L in the limit $L/\ell \gg 1$ to the hydrodynamic results calculated employing the boundary condition(1.1-2), the Onsager coefficients a, b, c have been determined. The slip length and thermal resistances are obtained by numerical calculations and also by analytic solutions in terms of Onsager coefficients.

Next, the case of ^4He has been discussed briefly. In ^4He case, the number of quasiparticles is not conserved in collisions, we can drop the chemical potential from the set of hydrodynamic variables relevant for time-independent flow. A rigorous bound for ratio $v_n(\infty)/\delta T_w$ is derived analytically and is in good agreement with the numerical result.

In the second part, we treat a nonstationary process. Since the time scale for electron collision in a semiconductor is typically in the subpicosecond range, the electron distributions are highly nonequilibrium within half of a picosecond from photoexcitation. Femtosecond spectroscopy is therefore an ideal tool for studying the dynamics of carrier scattering processes.^{29–31}

The femtosecond relaxation process in GaAs has received much attention in recent years because of its implication in the development of optical devices and the understanding of the carrier dynamics.^{32–35} Optical spectroscopy can, under the right circumstances, provide more direct information than electronic circuitry on certain electron scattering events, such as carrier-carrier, polar optic phonon, and intervalley because of limitations in electronic circuitry attributable to inherent RC time constants. In principle, time-independent electronic measurements such as the velocity-electric field curve provide information on these scattering mechanisms, but are usually averaged over both time and energy, therefore limiting quantitative comparisons of experiments and theory. In addition, the velocity-electric field curve is often dominated by impurity scattering, thus obscuring the effects of the other scattering mechanisms.

Interband absorption of light in semiconductors gives rise to photoexcited electrons with an energy $\epsilon_0 \simeq \hbar\omega_{ex} - \Delta$, where $\hbar\omega_{ex}$ is the energy of the exciting photon, and Δ is the gap width. These electrons are then scattered by impurities, majority carriers, and lattice vibrations, losing their initial energy and momentum in the process. The electrons may also recombine with holes in acceptor states. The combination time is usually several orders of magnitude longer than the scale time for energy and momentum relaxation. These excited

electrons determine the greater part of the photoluminescence spectrum during transitions from the conduction band to an acceptor level.

In recent spectroscopy experiments on bulk GaAs, by measuring the nonlinear optical transition, Rosker, Wise and Tang²⁹ investigated the relaxation of the photoexcited nonequilibrium electron distribution function in the optically coupled region (OCR) in k space. They found that the relaxation behavior can be described by a sum of exponentials with three characteristic time scales: a fast time component of $\sim 34fs$, an intermediate time component of $\sim 160fs$ and a long time component of $\sim 1600fs$. They suggested that $\Gamma \rightarrow L$ scattering along with electron-electron scattering is responsible for the fast process, polar optical phonon scattering is responsible for the intermediate time process, and a band-filling effect is responsible for the long time process.

In theoretically modeling femtosecond phenomena in semiconductor, the chief analytic tool is the well-known time-dependent Boltzmann transport equation.³⁶ Some of the first work done in understanding the femtosecond relaxation of carriers was of numerical solutions to the time-dependent Boltzmann equation for low energy excitations in bulk GaAs.³⁷ In Monte Carlo simulations, the solution of relaxation for high energy excitations³⁸ and the solution including intervalley scattering in GaAs³⁹ have been obtained and discussed in detail.⁴⁰

Monte Carlo approach has been emphasized in solving the semiconductor problems³ because of the difficulty and limitation of the exact analytical solutions. However Monte Carlo codes usually involve extensive amounts of preparation in writing, and require large-scale computational resources to run. The simulations are also subject to fluctuations inherent to any stochastic method. This makes it difficult to extract quantities from the simulations such as the

distribution function without noise, especially in regions where the number of particles is small. Increasing the number of particles can help, but only at the cost of increasing the amount of running time. Unequal weighting of simulation electrons can also be used to reduce fluctuations, but increases the complexity of the simulation.⁴⁰

In chapter 8, the band structure of bulk GaAs is described and the possible scattering mechanisms are reviewed. We will focus on the polar optic phonon scattering and the intervalley deformation potential scattering and neglect other scattering mechanisms. A general set of Boltzmann equations for a non-degenerate two valley system is given and the detailed balance conditions are discussed.

In chapter 9, a matrix method is introduced in solving a set of coupled Boltzmann equations. The problem is then converted to the solution of eigenvalues and eivenvectors of a large matrix with elements corresponding to the scattering kernels in rate equations.

The numerical excitation relaxation results are presented in chapter 10. The relaxation processes in fast and intermediate time scales are discussed. On a longer time scale, oscillations occur in the distribution functions and agree with those obtained from hot luminescence spectrum. The separation in energy between the peaks of the electron distribution in the conduction band clearly shows the role of polar optic phonon scattering in the relaxation processes.

Finally, in chapter 11, the results obtained are summarized and discussed.

CHAPTER 2 THERMAL TRANSPORT IN SUPERFLUID ^3He

2.1 Two Fluid Model

At room temperature ^3He is a harmless inert gas with nearly the same properties as the more common isotope ^4He , apart from the different mass. As one cools ^3He below its critical temperature of 3.3 K the gas condenses into a liquid, which behaves rather like a dense classical gas. On cooling further one finds that liquid ^3He (as well as ^4He), unlike all other known liquids, does not solidify unless a pressure of about 30 bar is applied. This is the first dramatic manifestation of macroscopic quantum effects in this system. The superfluid phases of ^3He were discovered in an experiment by Osheroff, Richardson and Lee⁴¹ in 1971. It is remarkable that a major part of the unusual phenomena so far observed in superfluid ^3He can be explained within a Landau-BCS-type mean field theory allowing for a complicated tensorial order parameter or off-diagonal mean field.^{42–48}

The properties of normal liquid ^3He in the temperature range from well below the Fermi temperature T_F of about 1 K to the transition temperature in the superfluid phases can be accounted for by the Landau Fermi liquid model.^{49–51} This model is based on the concept of elementary excitations according to which the low-energy properties of an interacting many-body system can be described in terms of a rarefield gas of elementary excitations or quasiparticles. Considering that in normal liquid ^3He the interparticle distance is comparable with the range of the interaction forces, interaction effects can be

expected to be very important. However at temperatures $T \ll T_F$ the relevant degrees of freedom are severely reduced by the Fermi statistics. The majority of particles are frozen into states deep in the Fermi sea. Only a fraction T/T_F of particles participate actively interaction processes.^{52,53}

The prediction of the existence of the superfluid state of liquid ^3He as well as many of its qualitative properties prior to the actual discovery can be considered a remarkable success of theoretical many-body physics.^{54–58} The framework of the model to be used is given by combining the concept of the normal Fermi liquid with the idea of pair correlations underlying the BCS theory.⁵⁹ This is done by treating the pair correlation as a perturbation on the Fermi liquid in the sense that only states within an energy shell $k_B T_c$ about the Fermi surface are appreciably affected. Following BCS, we may describe the condensed state by a properly antisymmetrised product of pair wavefunctions, keeping the important correlations within one pair, but treating the interaction between pairs in mean field theory. The single-particle excitations with momentum p , spin projection σ and energy $E_{p\sigma}$ are called Bogoliubov quasiparticles. A Bogoliubov quasiparticle is a coherent superposition of a normal quasiparticle and a quasihole. In contrast to normal quasiparticles the number of Bogoliubov quasiparticles is not conserved. The change in the quasiparticle spectrum induced by the off-diagonal mean field is obtained by the well known procedure.⁶⁰ The interaction between Cooper pairs in the system can be described by an off-diagonal mean field $\Delta_{p\sigma\sigma'}$ acting on the Cooper pair $(\mathbf{p}\sigma, -\mathbf{p}\sigma')$, given by the superposition of contributions from all other pairs

$$\Delta_{p\sigma\sigma'} = \sum_{p'} v_{pp'} g_{p'\sigma\sigma'} \quad (2.1)$$

where $v_{pp'}$ is the effective interaction between two quasiparticles on the Fermi surface with momenta \mathbf{p} , $-\mathbf{p}$ and \mathbf{p}' , $-\mathbf{p}'$ respectively, $g_{p\sigma\sigma'}$ is the probability amplitude for finding a Cooper pair with momenta and spins of the constituent quasiparticles($\mathbf{p}\sigma$, $-\mathbf{p}\sigma'$). The quasiparticle spectrum then is

$$E_p = (\xi_p^2 + \Delta_{\hat{p}}\Delta_{\hat{p}}^\dagger)^{\frac{1}{2}} \quad (2.2)$$

where $\xi_p = \epsilon_p - \mu$. In general E_p is 2×2 matrix in spin space. For the class of pairing states with Δ proportional to a unitary matrix, which seems to be realised for ${}^3\text{He}$ (in zero magnetic field), the matrix product $\Delta\Delta^\dagger$ in equation (2.2) is proportional to the unit matrix and E_p is independent of spin.

The energy spectrum described by equation (2.2) has a gap

$$|\Delta_{\hat{p}}| = [\frac{1}{2}\text{Tr}_\sigma(\Delta_{\hat{p}}\Delta_{\hat{p}}^\dagger)]^{\frac{1}{2}} \quad (2.3)$$

at the Fermi surface. $\Delta_{\hat{p}\sigma\sigma'}$ is therefore referred to as the gap parameter.

At finite temperatures the dominant thermal excitations will be Bogoliubov quasiparticles. Since the Bogoliubov quasiparticles are non-interacting fermions (within the mean field description) their distribution in momentum space is given by the fermi function

$$f_{p\sigma} = (e^{\beta E_p} + 1)^{-1} \quad (2.4)$$

where $\beta = (k_B T)^{-1}$

It turns out that the off-diagonal mean field conventionally called the gap parameter, is not determined uniquely by the usual self-consistency equation (gap equation) contrary to the case of s -wave pairing in superconductors. Comparison of the magnetic properties of the model states with experiment suggests the identification of the A phase with the so-called ABM (Anderson-

Brinkman-Morel) state^{46,54,55} and the B phase with the so-called BW (Balian-Werthamer)state.⁶¹ Both the ABM and BW order parameters are complex-valued, due to the $L = 1$ (p wave) and $s = 1$ (triplet) symmetry in orbital and spin space. The ABM state is axially symmetric in position space and spin space, and in particular the single-particle excitation spectrum is axially symmetry in momentum space. The BW state is isotropic with respect to simultaneous rotations in position space and spin space, but is anisotropic with respect to relative rotations of orbital and spin coordinates. Especially in the BW phase, the gap Δ in the dispersion relation is isotropic.

For many purposes it is legitimate to consider a pair-correlated Fermi liquid as consisting of two interpenetrating fluids, the fluid of cooper pairs and the fluid of Bogoluibov quasiparticles. The BCS transition may be thought of as a Bose-Einstein condensation of pairs. It shares the property of superfluidity with the genuine Bose-Einstein condensed state. Here the role of the superfluid component is played by the condensate of Cooper pairs, while the normal component is represented by the thermal excitations, most importantly the Bogoluibov quasiparticles. In fact the supercurrent structure is considerably more complicated than that of an ordinary superfluid,⁴⁷ but for many practical purposes we expect that the straight forward approach followed by Anderson and Morel,^{54,55} Balian and Werthamer,⁶¹ and later Saslow⁶² will suffice. Let us suppose that the quasiparticle fluid, or normal fluid, moves as a whole with velocity v_n , the energy of a quasiparticle with momentum p in the rest frame is given by

$$E_p(\mathbf{v}_n) = E_p - \mathbf{p} \cdot \mathbf{v}_n \quad (2.5)$$

The mass current carried by the normal fluid is

$$\mathbf{g}_n = \sum_{p\sigma} \mathbf{p} f(\mathbf{E}_p - \mathbf{p} \cdot \mathbf{v}_n) = \rho_n^o \cdot \mathbf{v}_n + o(\mathbf{v}_n^2) \quad (2.6)$$

where $\rho_{nij} = \sum_{p\sigma} p_i p_j (-\frac{\partial f}{\partial E_p})$ is the tensor of normal fluid density ($f(E)$ is the Fermi function).

Actually the thermal excitations do not move completely independent from the Cooper pairs. As in the normal state, a moving quasiparticle pushes aside the particles in its way, which in turn flow back to fill the hole behind the quasiparticle. This effect is described by the term in the Fermi liquid interaction involving F_1^s .

In the BW state ρ_n is isotropic,

$$\rho_n = \frac{(1 + \frac{1}{3} F_1^s) Y(T)}{1 + \frac{1}{3} F_1^s Y(T)} \quad (2.7)$$

Here $Y(T)$ is Yoshida's function

$$Y(T) = \int \frac{d\Omega_p}{4\pi} Y(\hat{p}, T) \quad (2.8)$$

and

$$Y(\hat{p}, T) = \frac{1}{4} \beta \int_{-\infty}^{\infty} d\xi_p \text{sech}^2(\frac{1}{2} \beta E_p) \quad (2.9)$$

At low temperatures,

$$\rho_n / \rho \simeq (m^*/m)(\pi\beta\Delta)^{\frac{1}{2}} \exp(-\beta\Delta) \quad (2.10)$$

In the ABM state the normal fluid density is anisotropic with respect to the axis of the gap $\hat{\ell}$. For simplicity we only consider the BW state in the following discussion.

The time evolution of the local quasiparticle distribution function $n_{p\sigma}(r, t)$ is described by the kinetic equation⁵⁰

$$\partial_t n_{p\sigma} + \nabla_p \epsilon_{p\sigma} \cdot \nabla_r n_{p\sigma} - \nabla_r \epsilon_{p\sigma} \cdot \nabla_p n_{p\sigma} = I\{n_{p\sigma}\} \quad (2.11)$$

The left hand side of equation (2.11) accounts for the continuous change of the distribution due to the streaming of quasiparticles in phase space. The collision integral I describes discontinuous changes brought about by collisions. The derivation of (2.11) is given in Appendix A. The comprehensive discussions of this theory are given in the articles by Baym and Pethick⁶³ and by P.Wölfle.⁶⁴ We will investigate this equation in the form related to the specific stationary problem involving boundary effects as follows.

2.2 Kinetic Equations

The dynamics of a weakly excited superfluid on length scales large as compared to the coherence length is described by a linearized Landau-Boltzmann equation for a distribution function of quasi-particles f_p , namely

$$v_{px} \frac{d}{dx} (\delta f_p - f'_p \delta E) = I_p \{ \delta f'_p \} \quad (2.12)$$

where v_{px} is the group velocity in the x direction, δf_p is the deviation of the distribution function from the global reference equilibrium, $f'_p = \frac{df_p}{dE_p}$ the derivative of the Fermi function with respect to the energy E , δE_p is the deviation of the quasiparticle energy from the equilibrium value given by equation(15) of Betbeder-Matibet and Nozières.⁶⁵ Actually, there is not needed any explicit expression for δE_p in the present static problem. I_p is the collision integral, which is a complicated function of the distribution, as derived by Einzel and Wölfle.⁶⁶ Here the simplest form of it is used, which satisfies the conservation laws and captures the essential physics of the problem. For this it can be written

$$I_p = I_{out} + I_{in} \quad (2.13)$$

where I_{out} is the ‘‘out scattering’’ collision integral, approximated by the single time relaxation approximation,

$$I_{out} = -\frac{\delta f_p'}{\tau} \quad (2.14)$$

Here $\delta f_p'$ is the deviation from the local equilibrium,

$$\delta f_p' = \delta f_p - f_p'(\delta E_p - p_x v_n(x) - E_p \frac{\delta T(x)}{T}) \quad (2.15)$$

where v_n and δT are the normal velocity and the deviation of the local temperature from the global equilibrium as defined quantitatively below, τ is the moment independent relaxation time. I_{in} is the ‘‘in scattering’’, in general very complicated and is worked out only for some particular transport problems by Wölfle and Einzel.⁶⁷ Doing an analogous task in this case is a formidable task. Instead the simplest I_{in} is used to produce at least qualitatively the physics. Extend the equation(35) of Ref.67 to the case of finite v_n and δT , thus

$$I_{in} = -\frac{1}{\tau} f_p' [p_x v_n(x) + E_p \frac{\delta T(x)}{T} + \frac{\xi_p}{E_p} \delta \mu_n(x)] \quad (2.16)$$

where

$$\delta \mu_n(x) = -\sum_{p'} \frac{\xi_p'}{E_p'} \delta f_{p'} / \sum_{p'} f_{p'} \quad (2.17)$$

here $\xi_p = (p - p_F)v_F$ is the normal state quasiparticle energy measured from the chemical potential. The energy of the quasiparticles is $E_p = (\xi_p^2 + \Delta^2)^{\frac{1}{2}}$

The simplest form of the collision integral obeying the conservation laws means that it involves only the deviation from local equilibrium. Defining

$$\delta f_p'' \equiv \delta f_p' + f_p' [p_x v_n(x) + E_p \frac{\delta T(x)}{T} + \frac{\xi_p}{E_p} \delta \mu_n] \quad (2.18)$$

(2.12) becomes

$$v_{p_x} \frac{\partial}{\partial x} [\delta f_p'' - f_p' Q_p(x)] = -\frac{\delta f_p''}{\tau} \quad (2.19)$$

where

$$Q_p(x) = p_x v_n(x) + \frac{\xi_p}{E_p} \delta\mu_n(x) + E_p \frac{\delta T(x)}{T} \quad (2.20)$$

This linear equation can be simply solved,

$$\delta f_p^{(+)}(x) = c_1 e^{-\lambda_p^{-1}x} + \int^x dx' e^{-\lambda_p^{-1}(x-x')} f_p' \frac{dQ_p(x')}{dx'} \quad (2.21)$$

$$\delta f_p^{(-)}(x) = c_2 e^{+\lambda_p^{-1}x} + \int^x dx' e^{-\lambda_p^{-1}(x'-x)} f_p' \frac{dQ_p(x')}{dx'} \quad (2.22)$$

where $\lambda_p = |v_{p_x}| \tau$, a ‘‘projected’’ mean free path. Here \pm specifies whether $v_{p_x} > 0$ or $v_{p_x} < 0$. c_1, c_2 are integration constants. These as well as the lower limits of the integrations are determined by the boundary conditions. The ‘‘half space’’ case (half infinite geometry) and the ‘‘sandwich’’ case (parallel plates geometry), as shown in Fig.1, are treated separately as follows.

2.3 Solution for Half Space Case

Assume that the wall is at $x = 0$, with the superfluid occupying $x > 0$, the quasiparticles scatter diffusely, i.e. emerging at local equilibrium with the wall. The corresponding distribution function for $v_{p_x} > 0$ is

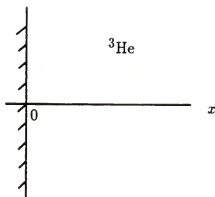
$$f_p^{(+)}(0) = f((E_p + \delta E_p)/(T + \delta T_L)) \quad (2.23)$$

where $f(x) \equiv (e^x + 1)^{-1}$, δT_L is the deviation of the wall temperature from the global equilibrium one, which is taken to be the temperature at $x = \infty$, i.e., $\delta T(x \rightarrow \infty) \rightarrow 0$. Thus by (2.18)(see Appendix C),

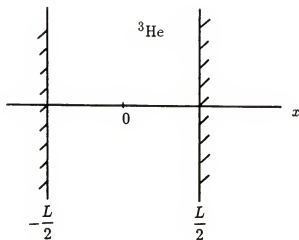
$$\delta f_p^{(+)}(0) = f_p'(p_x v_n(0) + \frac{\xi_p}{E_p} \delta\mu_n(0) + E_p \frac{\delta T(0) - \delta T_L}{T}) \quad (2.24)$$

The solution of the kinetic equation is therefore

$$\delta f_p^{(+)}(x) = e^{-\lambda_p^{-1}x} \delta f_p^{(+)}(0) + \int_0^x dx' e^{-\lambda_p^{-1}(x-x')} f_p' \frac{dQ_p(x')}{dx'} \quad (2.25)$$



${}^3\text{He}$ in half infinite geometry (half space).



${}^3\text{He}$ between parallel plates (sandwich case).

FIG. 1. ${}^3\text{He}$ in half infinite geometry (half space case) and between parallel plates (sandwich case).

$$\delta f_p^{(-)}(x) = \int_{-\infty}^x dx' e^{-\lambda_p^{-1}(x'-x)} f_p' \frac{dQ_p(x')}{dx'} \quad (2.26)$$

To obtain the profiles of $\delta T(x)$, $v_n(x)$ and $\delta\mu_n(x)$, we shall make use of the conservation laws of momentum and energy, together with the definition of $\delta\mu_n$ in (2.17).

(a) Momentum conservation

Notice the fact that either side of equation (2.19), when multiplied by p_x and summed over all p , vanishes identically. In particular, by considering the left hand side,

$$c_m = \sum_p p_x v_{p_x} (\delta f_p''(x) - f_p' Q_p(x)) \quad (2.27)$$

where c_m is an x -independent constant.

It is intuitively reasonable that the quasiparticles will approach local equilibrium as $x \rightarrow \infty$. Thus $\delta f_p'(x) \rightarrow 0$ as $x \rightarrow \infty$, and so does $\delta f_p''(x)$ by (2.18). It is also clear that $v_n(x) \rightarrow v_n(\infty) = \text{constant}$, and by definition $\delta T(\infty) \rightarrow 0$. From (2.17) $\delta\mu_n(\infty) \rightarrow 0$ also. Substituting these results in (2.27) and noticing the appropriate symmetries, c_m can be obtained to be equal to zero. It is convenient to break the sum into $v_{p_x} > 0$ and $v_{p_x} < 0$ parts, and substitute the solution for $\delta f_p''(x)$ to (2.27). For the $v_{p_x} < 0$ part, relabel the dummy $\vec{p} = -\vec{p}$. The integral kernels are defined by

$$\begin{pmatrix} K_n(x) \\ L_n(x) \\ M_n(x) \\ N_n(x) \\ P_n(x) \\ Q_n(x) \end{pmatrix} = \sum_{\substack{\vec{p} \\ v_{p_x} > 0}} (-f_p') v_{p_x} \lambda_p^{n-1} e^{-\lambda_p^{-1}x} \begin{pmatrix} p_x^2 \\ p_x \frac{\xi_p}{E_p} \\ p_x E_p \\ \frac{\xi_p^2}{E_p} \\ E_p^2 \\ 1 \end{pmatrix} \quad (2.28)$$

The kernels satisfy the relations

$$\frac{dL_n(x)}{dx} = -L_{n-1}(x), \text{ etc.} \quad (2.29)$$

and

$$\int_0^{\infty} dx' L_0(|x - x'|) = 2L_1(0) - L_1(x) \quad (2.30)$$

Then, the equation (2.27) can be written as

$$\begin{aligned} 0 = & -K_1(x)v_n(0) - L_1(x)\delta\mu_n(0) - M_1(x)\frac{\delta T(0) - \delta T_L}{T} \\ & - \int_0^x dx' [K_1(x-x')\frac{dv_n(x')}{dx'} + L_1(x-x')\frac{d\mu_n(x')}{dx'} + M_1(x-x')\frac{1}{T}\frac{dT(x')}{dx'}] \\ & - \int_{\infty}^x dx' [-K_1(x'-x)\frac{dv_n(x')}{dx'} + L_1(x-x')\frac{d\mu_n(x')}{dx'} + M_1(x-x')\frac{1}{T}\frac{dT(x')}{dx'}] \\ & + 2L_1(0)\delta\mu_1(x) + 2M_1(0)\frac{\delta T(x)}{T} \end{aligned} \quad (2.31)$$

The integrals involving K_1 can be collected to form $-\int_0^{\infty} dx' K_1(|x-x'|)\frac{dv_n(x')}{dx'}$, the others can be integrated by parts, e.g., for the ones involving L

$$\begin{aligned} & - \int_0^x dx' L_1(x-x')\frac{d\mu_n(x')}{dx'} - \int_{\infty}^x dx' L_1(x-x')\frac{d\mu_n(x')}{dx'} \\ & = -2L_1(0)\delta\mu_n(x) + L_1(x)\delta\mu_n(0) + \int_0^{\infty} dx' L_0(|x-x'|)\delta\mu_n(x') \end{aligned} \quad (2.32)$$

where the relation of $\frac{dL_1(x)}{dx} = -L_1(x)$ has been used. After manipulating similarly the terms involving M, it can be obtained that

$$\begin{aligned} 0 = & -K_1(x)v_n(0) + M_1(x)\frac{\delta T_L}{T} - \int_0^{\infty} dx' [K_1(|x-x'|)\frac{dv_n(x')}{dx'} \\ & - L_0(|x-x'|)\delta\mu_n(x') - M_0(|x-x'|)\frac{\delta T(x')}{T}] \end{aligned} \quad (2.33)$$

(b) Energy conservation

Either side of equation (2.19), when multiplied by E_p and summed over all \vec{p} , is zero. In particular the left hand side yields

$$c_E = \sum_p E_p v_{pz} [\delta f_p'' - f_p'(p_x v_n(x) + \frac{\xi_p}{E_p} \delta\mu_n(x) + E_p \frac{\delta T}{T})] \quad (2.34)$$

where c_E is a constant, similar to the discussion in momentum conservation, it is obtained that

$$c_E = \sum_p E_p v_{p_x} (-f'_p) p_x v_n(\infty) = 2M_1(0)v_n(\infty) \quad (2.35)$$

by carrying out a similar procedure as in (a). Assume that the sum $\sum_{p, v_{p_x}} v_{p_x} \xi_p$ vanishes by particle-hole symmetry. This is because the contributions to the summation from $\vec{v}_{p_x 1} = \vec{v}_{p_x 2}$, cancel each other. The resulting equation reads

$$2M_1(0)v_n(\infty) = -P_1(x) \frac{\delta T(0) - \delta T_L}{T} + \int_0^\infty dx' [M_0(|x - x'|)v_n(x') - P_1(|x - x'|) \frac{1}{T} \frac{dT(x')}{dx}] \quad (2.36)$$

(c) Definition of pseudo-chemical potential

In a normal Fermi system the number of quasiparticles is conserved in collisions. But as one passes through the transition into the superfluid state, the quasiparticle number conservation law is gradually relaxed. This gives a quasi-conservation law for the number of excitations. Hence, even though the chemical potential is not a hydrodynamic variable in the strict sense, it can still be taken as a quasi-hydrodynamic variable.

On the other hand, the coupling of thermal and mechanical variables in a degenerate Fermi system is greatly reduced by the Pauli principle. In the temperature region near T_c one may therefore expect the effects of the local temperature on the velocity field to be dominated by the influence of the quasiconservation law involving the chemical potential.

Equation (2.17) can be rewritten with the help of (2.18) as

$$\sum_p (-f'_p) \delta \mu_n(x) = \sum_p \frac{\xi_p}{E_p} (\delta f''_p(x) - f'_p \frac{\xi_p}{E_p} \delta \mu_n(x)) \quad (2.37)$$

Considering that particle hole symmetry implies $\sum_{p, v_{px} > 0} \xi_p = 0$, we finally get

$$2Q_0(0)\delta\mu_n(x) = -L_0(x)v_n(0) - \int_0^\infty dx' [L_0(|x-x'|)\frac{dv_n(x')}{dx'} - N_{-1}(|x-x'|)\delta\mu_n(x')] \quad (2.38)$$

The three coupled integro-differential equations (2.33),(2.36) and (2.38) can be solved numerically to obtain $\delta T(x)$, $\delta\mu_n(x)$ and $v_n(x)$ which will be presented in chapter 4. The analogous discussion for ‘‘sandwich’’ case is as follows.

2.4 Solution for Sandwich Case

We consider two walls at $\pm\frac{L}{2}$, at temperature differences $\delta T_R = -\delta T_L$ from our reference equilibrium temperature T , chosen to be that at $x = 0$. It can be seen as discussed in the last section that the boundary conditions for diffuse scattering are

$$\delta f_p^{''(+)}\left(-\frac{L}{2}\right) = f_p'(p_x v_n\left(-\frac{L}{2}\right) + \frac{\xi_p}{E_p} \delta\mu_n\left(-\frac{L}{2}\right) + E_p \frac{\delta T\left(-\frac{L}{2}\right) - \delta T_L}{T} \quad (2.39)$$

$$\delta f_p^{''(-)}\left(\frac{L}{2}\right) = f_p'(p_x v_n\left(\frac{L}{2}\right) + \frac{\xi_p}{E_p} \delta\mu_n\left(\frac{L}{2}\right) + E_p \frac{\delta T\left(\frac{L}{2}\right) - \delta T_R}{T} \quad (2.40)$$

here T_L and T_R are the temperatures of the left side wall and right side wall, again \pm distinguish $v_{p_x} > 0$ and $v_{p_x} < 0$. Thus our solution to the kinetic equation reads

$$\delta f_p^{''(+)}(x) = e^{-\lambda_p^{-1}(x+\frac{L}{2})} \delta f_p^{''(+)}\left(-\frac{L}{2}\right) + \int_{-\frac{L}{2}}^x dx' e^{-\lambda_p^{-1}(x-x')} f_p' \frac{dQ_p(x')}{dx'} \quad (2.41)$$

$$\delta f_p^{''(-)}(x) = e^{-\lambda_p^{-1}(x-\frac{L}{2})} \delta f_p^{''(-)}\left(\frac{L}{2}\right) + \int_{\frac{L}{2}}^x dx' e^{-\lambda_p^{-1}(x'-x)} f_p' \frac{dQ_p(x')}{dx'} \quad (2.42)$$

Consider the conservation laws and the definition of $\delta\mu_n(x)$ to derive three coupled integral equations:

(a) Momentum conservation

$$\sum_p p_x v_{p_x} (\delta f_p'' - f_p' Q_p(x)) = const \quad (2.43)$$

Using a similar derivation as for the half space case, and doing integration by parts like

$$\begin{aligned} & - \int_{-\frac{L}{2}}^x dx' L_1(x-x') \frac{d\mu_n(x')}{dx'} - \int_{\frac{L}{2}}^x dx' L_1(x'-x) \frac{d\mu_n(x')}{dx'} \\ & = -2L_1(0)\delta\mu_n(x) + L_1(x + \frac{L}{2})\delta\mu_n(-\frac{L}{2}) \\ & + \int_{-\frac{L}{2}}^{\frac{L}{2}} dx' L_0(|x-x'|)\delta\mu_n(x) \end{aligned} \quad (2.44)$$

we obtain the momentum conservation equation

$$\begin{aligned} & -K_1(x + \frac{L}{2})v_n(-\frac{L}{2}) + K_1(\frac{L}{2} - x)v_n(\frac{L}{2}) + M_1(x + \frac{L}{2})\frac{\delta T_L}{T} \\ & + M_1(\frac{L}{2} - x)\frac{\delta T_R}{T} + \int_{-\frac{L}{2}}^{\frac{L}{2}} dx' [-K_1(|x-x'|)\frac{dv_n(x')}{dx'} \\ & + L_0(|x-x'|)\delta\mu_n(x') + M_0(|x-x'|)\frac{\delta T(x')}{T}] = const \end{aligned} \quad (2.45)$$

(b) Energy conservation

By considering

$$\sum_p E_p v_{p_x} (\delta f_p'' - f_p' Q_p(x)) = const \quad (2.46)$$

as in the above, we find

$$\begin{aligned} & -P_1(x + \frac{L}{2})\frac{\delta T(-\frac{L}{2}) - \delta T_L}{T} + P_1(-x + \frac{L}{2})\frac{\delta T(\frac{L}{2}) - \delta T_R}{T} \\ & + \int_{-\frac{L}{2}}^{\frac{L}{2}} dx' [M_0(|x-x'|)v_n(x') - P_1(|x-x'|)\frac{dT(x')}{T dx'}] = const \end{aligned} \quad (2.47)$$

The constant can be determined by putting $x = 0$ in the left side, thus we get

$$\begin{aligned}
& - [P_1(x + \frac{L}{2}) - P_1(\frac{L}{2})] \frac{\delta T(-\frac{L}{2}) - \delta T_L}{T} \\
& + [P_1(-x + \frac{L}{2}) - P_1(\frac{L}{2})] \frac{\delta T(\frac{L}{2}) - \delta T_R}{T} \\
& + \int_{-\frac{L}{2}}^{\frac{L}{2}} dx' \{ [M_0(|x - x'|) - M_0(|x'|)] v_n(x') \\
& - [P_1(|x - x'|) - P_1(|x'|)] \frac{dT(x')}{T dx'} \} = 0
\end{aligned} \tag{2.48}$$

(c) Definition of pseudo-chemical potential

Using the definition of $\delta\mu_n(x)$ and the solution for $\delta f_p''(x)$, we get

$$\begin{aligned}
2Q_1(0)\delta\mu_n(x) &= -L_0(x + \frac{L}{2})v_n(-\frac{L}{2}) + L_0(\frac{L}{2} - x)v_n(\frac{L}{2}) \\
& - \int_{-\frac{L}{2}}^{\frac{L}{2}} dx' [L_0(|x - x'|) \frac{dv_n(x')}{dx'} - N_{-1}(|x - x'|)\delta\mu_n(x')]
\end{aligned} \tag{2.49}$$

There are some useful symmetry relations in this problem. For linearized solution, it is obvious that the deviations of the wall temperature from the reference at $x = 0$ are equal but opposite: $\delta T_L = -\delta T_R$ and $\delta T(x)$ is an odd function of x . By considering the heat transfer it is also clear that $v_n(x)$ must be even in x . A glance at the integral equations will show that $\delta\mu_n(x)$ must be odd in x .

Alternatively we can consider the problem via the kinetic equations. It is clear that when the wall temperatures are equal and opposite, by considering an inversion $x = -x$, one must have $\delta f_p(x) = \delta f_{-p}(-x)$, and by (2.15) and (2.18), $\delta f_p'$ and $\delta f_p''$ must have the same properties. In summary,

$$\begin{aligned}
v_n(x) &= v_n(-x) \\
\delta T(x) &= -\delta T(-x) \\
\delta\mu_n(x) &= -\delta\mu_n(-x) \\
\delta f_p^{''(+)}(x) &= \delta f_{-p}^{''(-)}(-x)
\end{aligned} \tag{2.50}$$

with those, the constant in (2.45) equals zero. The symmetry will allow us to decrease the computation time considerably.

CHAPTER 3 HYDRODYNAMIC LIMIT

3.1 Hydrodynamic Description

When hydrodynamics is applicable to the superfluid ${}^3\text{He}$ between two parallel plates and in the presence of a stationary heat flow normal to the plates, as explained in Ref.22 and 23, the macroscopic quantities of the system, in particular the deviation of the temperature from equilibrium, depend on position x with a characteristic length scale $\lambda = (Ts^2/\kappa\alpha)^{-\frac{1}{2}}$ in the static limit, here T is the temperature, s is the entropy density, $\alpha = \frac{4}{3}\eta - 2\zeta_1\rho + \zeta_2 + \zeta_3\rho^2$ is a combination of viscosity coefficients⁶⁸, κ is the thermal conductivity. Two other relevant length scales are the size of experimental cell L and the mean free path $\ell(T)$ of the Bogoliubov quasiparticles. Notice that hydrodynamics does not apply within a few $\ell(T)$ near the wall. Whether there is coupling between the walls (i.e. when the sandwich problem does not degenerate into two half-space problems) depends on whether $L > \lambda$ or $L < \lambda$. From the known expressions of the thermodynamic and transport coefficients,⁶⁷ we have calculated λ/ℓ for ${}^3\text{He-B}$. The result is given in Fig.2. One can see that λ is large as $T \rightarrow 0$ or T_c , the former is mainly due to the exponential increase of ℓ , the latter is due to the divergence of the second viscosity coefficients, and one sees that $\lambda/\ell \gg 1$ always. Thus we have three possible limiting regimes:

(1) $L \gg \lambda \gg \ell$ In this case hydrodynamics applies to a large region of x , and since the deviation of temperature from equilibrium, for example, decays exponentially away from the wall, and since $L \gg \lambda$, the walls are practically

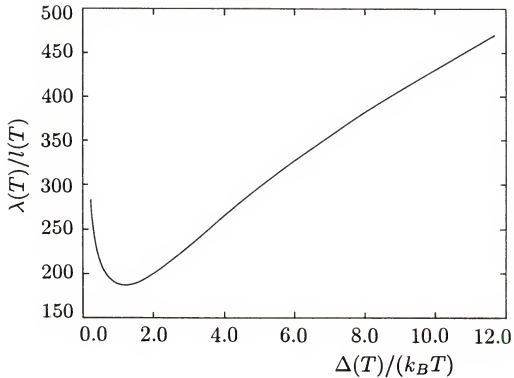


FIG. 2. The ratio of the thermal decay length $\lambda(T)$ to the mean free path $l(T)$ as a function of temperature. Plotted is the normalized quantity $\lambda(T)/l(T)$ vs $\Delta(T)/(k_B T)$.

decoupled. In this case the calculations in the two geometries yield the same information, and are relevant for large sample size and relatively high temperatures (except when $T \rightarrow T_c$ where λ diverges)

(2) $\lambda \geq L \gg \ell$ Most realistic experiments of ^3He fall into this regime. While hydrodynamics applies to the appropriate regime in space, the walls are coupled via the sq-mode. The sandwich calculation is directly applicable to this case. Fitting the solution to the hydrodynamic equations with the boundary condition (1.1-2) to the numerical solution, the values of the Onsager coefficients are obtained. This is the relevant regime at intermediate temperatures and a narrow region of T as $T \rightarrow T_c$.

(3) $\ell > L$ In this so-called Knudsen regime hydrodynamics simply fails, and the direct solution of the sandwich problem is necessary. This is always the case at sufficiently low temperatures, when $\ell(T)$ diverges. In this case the analysis of Ref.22 and 23 does not apply, and the calculation should be compared directly with the experiment.

In ^4He since λ is not a hydrodynamic length ($\sim \ell$) except in a critical ($T \rightarrow T_c$) region one only needs to distinguish the cases of $L > \ell$ or $L < \ell$.

To make connections of the microscopic description with hydrodynamic equations of Khalatnikov,²⁴ the superfluid hydrodynamics in the linear regime is recalled as follows.

The momentum conservation implies, in this static problem

$$\frac{dP(x)}{dx} - \left(\frac{4}{3}\eta - 2\zeta_1\rho + \zeta_2 + \zeta_3\rho^2\right)\frac{d^2v_n(x)}{dx^2} = 0 \quad (3.1)$$

where P is the pressure. The fact that the superfluid velocity is time independent requires, at zero mass flow,

$$\frac{\partial}{\partial x}(\mu + \zeta_3\rho\frac{\partial v_n}{\partial x}) = 0 \quad (3.2)$$

here η is the coefficient of shear viscosity, ζ_1 , ζ_2 and ζ_3 are coefficients of second viscosity. It follows from the microscopic theory that ζ_1 and ζ_2 are small, of the order of $(T_c/T_F)^2$ and may be neglected,^{69,70} μ is the thermodynamic chemical potential (it is different from the pseudo-chemical potential defined in the last chapter), related to the pressure and temperature by the thermodynamic relation

$$d\mu = -\frac{s}{\rho}dT + \frac{1}{\rho}dP \quad (3.3)$$

Combining (3.1), (3.2) and (3.3) gives

$$s\frac{dT}{dx} - \left(\frac{4}{3}\eta + \zeta_3\rho^2\right)\frac{d^2v_n}{dx^2} = 0 \quad (3.4)$$

The energy flux, on the other hand, gives

$$f = sv_n - \frac{\kappa}{T}\frac{dT}{dx} \quad (3.5)$$

where f is a constant. The thermal decay length can be obtained from (3.4) and (3.5),

$$\lambda^{-2} = Ts^2/\kappa\alpha \quad (3.6)$$

here $\alpha = \frac{4}{3}\eta + \zeta_3\rho^2$. Now under the approximation for the collision integral, from Ref.67, the expression for the transport coefficients can be defined as

$$\langle A \rangle = \int_{-\infty}^{\infty} d\xi (-f'(E))A(\xi) \quad (3.7)$$

we have

$$\eta = \frac{p_F^4 v_F}{15\pi^2 \hbar^3} \langle \tau \frac{\xi^2}{E^2} \rangle \quad (3.8)$$

$$\kappa = \frac{p_F^2 v_F}{3\pi^2 \hbar^3 T} \langle \tau \xi^2 \rangle \quad (3.9)$$

$$\zeta_3\rho^2 = \frac{p_F^4 v_F}{9\pi^2 \hbar^3} \left[\langle \tau \frac{\xi^2}{E^2} \rangle + \frac{\langle \xi^2/E^2 \rangle^2}{\langle \Delta^2/E^2 \tau \rangle} \right] \quad (3.10)$$

The entropy density is given by

$$s = -k_B \frac{p_F^2}{\pi^2 \hbar^3 v_F} \int_{-\infty}^{\infty} d\xi \left[\ln \frac{e^{E/k_B T}}{e^{E/k_B T} + 1} - \frac{E}{k_B T} \frac{1}{e^{E/k_B T} + 1} \right] \quad (3.11)$$

After partial integrations, the entropy expression can be rewritten as

$$s = \frac{1}{\pi^2 \hbar^3} \frac{p_F^2}{v_F T} \langle \xi^2 \rangle \quad (3.12)$$

3.2 Hydrodynamic Limit Approach

To approach the hydrodynamic limit, we consider the equations in the last chapter (2.33),(2.36),(2.38) and (2.45),(2.48),(2.49) for x values which are at least a few mean free paths away from the walls. We notice that the kernels defined in (2.28) are functions of x with a length scale of order, or shorter than $v_F \tau$, where v_F is the Fermi velocity. Thus all these kernels have a range of order of $\ell(T)$ only. On the other hand, provided $|x| \gg \ell(T)$ in the half-space problem or $|x - \frac{L}{2}|, |x + \frac{L}{2}| \gg \ell(T)$ in the sandwich problem, one expects that the macroscopic quantities $\delta T(x)$, $v_n(x)$, $\delta \mu_n(x)$ are relatively smooth functions of x on the scale of $\ell(T)$. Applying the above observations to coupled equations in the half space and sandwich cases, the macroscopic quantities $\delta T(x)$, $\frac{dv_n(x)}{dx}$, $\delta \mu_n(x)$ can be expanded in Taylor series about $x' = x$. The lowest order terms involve only integrals of the kernels, and can be done exactly.

One can see that the terms of the next order in the expansion integrate to exponentially small terms (in the ratio of the distance of x from the wall to $\ell(T)$), and the next higher order terms integrate to terms with a smaller factor $(\ell/\lambda)^2$. We have then

$$-2K_2(0) \frac{dv_n(x)}{dx} + 2L_1(0) \delta \mu_n(x) + 2M_1(0) \frac{\delta T(x)}{T} = 0 \quad (3.13)$$

$$2M_1(0)v_n(x) - 2P_2(0)\frac{1}{T}\frac{dT(x)}{dx} = c_b \quad (3.14)$$

$$2L_1(0)\frac{dv_n(x)}{dx} + 2(Q_0(0) - N_0(0))\delta\mu_n(x) = 0 \quad (3.15)$$

for both the half space and the sandwich geometries. The pseudo-chemical potential $\delta\mu_n$ can be eliminated from the above equations, yielding

$$2M_1(0)\frac{\delta T(x)}{T} - [2K_2(0) + \frac{2(L_1(0))^2}{Q_0(0) - N_0(0)}]\frac{dv_n(x)}{dx} = 0 \quad (3.16)$$

(3.14) and (3.16) have exact analog in superfluid hydrodynamics. To see this examining the kernel integrals (2.28)

From the kernel integrals (2.28), one can easily find

$$K_2(0) = \frac{p_F^4 v_F}{10\pi^2 \hbar^3} \langle \tau \frac{\xi^2}{E^2} \rangle \quad (3.17)$$

$$L_1(0) = \frac{p_F^3}{6\pi^2 \hbar^3} \langle \frac{\xi^2}{E^2} \rangle \quad (3.18)$$

$$P_2(0) = \frac{p_F^2 v_F}{6\pi^2 \hbar^3} \langle \xi^2 \tau \rangle \quad (3.19)$$

$$Q_0(0) = \frac{p_F^2}{2\pi^2 \hbar^3} \frac{1}{v_F} \langle \frac{1}{\tau} \rangle \quad (3.20)$$

$$N_0(0) = \frac{p_F^2}{2\pi^2 \hbar^3} \frac{1}{v_F} \langle \frac{1}{\tau} \frac{\xi^2}{E^2} \rangle \quad (3.21)$$

For $M_1(0)$ one needs to be more careful. For this purpose the integral over the magnitude of p is converted to an integral over ξ , with $p = p_F + \frac{\xi}{v_F}$, since the integral is restricted to be near $\xi = 0$ by the f_p' factor. Taking the limits of ξ to $\pm\infty$, then substituting $\xi \rightarrow -\xi$ in the integral with $\xi < 0$, then

$$M_1(0) = \frac{1}{4\pi^2 \hbar^3} \frac{2}{3} \int_0^\infty d\xi (-f_p') [\xi(p_F + \frac{\xi}{v_F})^3 - \xi(p_F - \frac{\xi}{v_F})^3]$$

This result can be expressed as

$$M_1(0) = \frac{p_F^2}{2\pi^2 \hbar^3 v_F} \langle \xi^2 \rangle \quad (3.22)$$

Using these formula one sees immediately that (3.16) is just (3.4) (both are momentum conservation laws) and (3.14) is just (3.5) (energy conservation law). We thus have proven that our results reduce to the hydrodynamic ones in the appropriate limits (for appropriate values of x).

3.3 Thermal Decay Length

Having shown the validity of the hydrodynamic equations, the solution can be directly written down when the hydrodynamic limit applies. From (3.14) and (3.16), it can be obtained

$$\frac{d^2 T}{dx^2} - \frac{M_1^2(0)}{P_2(0)(K_2(0) - \frac{L_1^2(0)}{Q_0(0) - N_0(0)})} \delta T = 0 \quad (3.23)$$

The temperature T and normal velocity v_n in the static limit according to hydrodynamics⁷¹

$$\delta T = T_s^- e^{x/\lambda} + T_s^+ e^{-x/\lambda} \quad (3.24)$$

We obtain

$$\lambda^{-2} = \frac{2\gamma}{(v_F \tau)^2} \left(\frac{k_B T}{p_F v_F} \right)^2 \frac{\langle (\xi/k_B T)^2 \rangle}{\langle (\xi/E)^2 \rangle + \frac{9}{\langle (\Delta/E)^2 \rangle}} \quad (3.25)$$

This result is just the same as that obtained from hydrodynamic expression $\lambda^{-2} = \frac{T_s^2}{\kappa \alpha}$.

For the half space, with the wall at $x = 0$, the temperature and the normal velocity approach their $x \rightarrow \infty$ value exponentially with the same length scale λ .

$$\delta T(x) = T_s^+ e^{-x/\lambda} \quad (3.26)$$

$$v_n(x) = v_n(\infty) + \gamma e^{-x/\lambda} \quad (3.27)$$

here $\gamma = v_n(0) - v_n(\infty)$. Inspection of (3.15) shows that $\delta\mu_n(x)$ also approaches zero with the same length scale

$$\delta\mu_n(x) = \delta\mu_n(0)e^{-x/\lambda} \quad (3.28)$$

The coefficients T_s^+ and γ can be related to f_0 via the a, b, c coefficients, which have been introduced by Grabinski and Liu.^{22,23}

For the sandwich case one can proceed similarly to find the solution to the hydrodynamic approach as

$$\delta T(x) = 2T_s^- \sinh\left(\frac{x}{\lambda}\right) \quad (3.29)$$

$$v_n(x) = v_n(0) + \left(-\frac{2\kappa T_s^-}{T_s \lambda}\right) \left(1 - \cosh\left(\frac{x}{\lambda}\right)\right) \quad (3.30)$$

Accordingly, the temperature profile across a solid wall shows a jump at the wall, followed by an exponential decay regime of length λ .

CHAPTER 4 NUMERICAL SOLUTIONS

4.1 Half Space Case

In this chapter the numerical solutions to the kinetic equations for ${}^3\text{He}$ in the half space case and the sandwich case are obtained. For the half space case, the coupled equations (2.33), (2.36), (2.38) can be solved by standard matrix method. The integration in the coupled equations is divided into N subregional integrations and the whole integration equals the summation of N subregional integrations. In the numerical calculation for the half space case, several aspects should be considered, (i) a cut off in the spacial integration at some value x_M is introduced, (ii) the value $v_n(\infty)$ in (2.36) is not a given value and should be determined by our calculation, (iii) the kernel $N_{-1}(|x - x'|)$ in (2.38) is divergent as $x \rightarrow x'$.

To resolve these difficulties, notice that when $x_M \gg \ell(T)$, we are in the hydrodynamic regime and the hydrodynamic solution (3.13-15) applies near x_M . Therefore, if h is the discretization interval and j is an integer, from (3.27) we obtain

$$v_n(x_M - jh) = v_n(\infty) - (v_n(\infty) - v_n(x_M))e^{jh/\lambda} \quad (4.1)$$

or

$$v_n(\infty) = v_n(x_M) + \frac{v_n(x_M) - v_n(x_M - jh)}{e^{jh/\lambda} - 1} \quad (4.2)$$

To improve numerical accuracy we typically use $j = 1, 2, 3, 4$ and take the average. Thus the information which is needed for the $x > x_M$ regime is “folded” back to $x < x_M$. The discretization then results in a closed set of linear equations, and is solved by a simple inversion.

In order to treat the singularity of kernel $N_{-1}(|x - x'|)$ properly, the integral is divided into N subregional integrals, for example

$$\begin{aligned} & \int_0^{\infty} dx' M_0(|x - x'|) \frac{\delta T(x')}{T} \\ &= - \int_0^x dx' M_0(|x - x'|) \frac{\delta T(x')}{T} - \int_x^{\infty} dx' M_0(|x - x'|) \frac{\delta T(x')}{T} \end{aligned} \quad (4.3)$$

After discretization, then

$$\begin{aligned} & \int_0^{\infty} dx' M_0(|x - x'|) \frac{\delta T(x')}{T} \\ &= - \sum_{0 < \delta < \delta'} \int_{\delta'}^{\delta' + h} d\delta'' M_0(\delta - \delta'') \frac{\delta T(\delta'')}{T} \\ &\quad - \sum_{\delta < \delta'' < 1} \int_{\delta'}^{\delta' + h} d\delta'' M_0(\delta'' - \delta) \frac{\delta T(\delta'')}{T} \end{aligned} \quad (4.4)$$

and thus only the kernel parts are integrated and the approximation $\delta T(\delta'') = (\delta T(\delta' + h) + \delta T(\delta'))/2$ is used. By using (2.29), (4.4) becomes

$$\begin{aligned} & \int_0^{\infty} dx' M_0(|x - x'|) \frac{\delta T(x')}{T} \\ &= \sum_{0 < \delta < \delta'} [M_1(\delta - (\delta' + h)) - M_1(\delta - \delta')] \frac{\delta T(\delta' + h) + \delta T(\delta')}{2T} \\ &\quad + \sum_{\delta < \delta'' < 1} [M_1(\delta' + h - \delta) - M_1(\delta' - \delta)] \frac{\delta T(\delta' + h) + \delta T(\delta')}{2T} \end{aligned} \quad (4.5)$$

In this way the integral of kernel $N_{-1}(|x - x'|)$ is converted to the summation of $N_0(|x - x'|)$ terms, which are convergent in the calculation region. Then the singularity of $N_1(|x - x'|)$ is now treated exactly.

The results for the half space calculation at $T/T_c = 0.85$ are shown in Fig.3. Due to the limit of the numerical calculation capacity, the discretization of space stops at $x = 40\ell(T)$, $\ell(T)$ is defined as $\ell(T) = [\sum_p (v_p \tau)^2 f_p / \sum_p f_p]^{1/2}$. Further we simply take $\ell(T) = \ell(T_c) e^{\Delta/k_B T}$, and the “extrapolation” discussed above is used. All the material constants are from Ref.72. The comparison of the numerical result and the hydrodynamic limit which is obtained by fitting the relation of (3.26) to the numerical data far away from the boundary is shown in Fig.4. The hydrodynamic limits are well-obeyed a few $\ell(T)$ away from the wall. $\delta T(x), v_n(x)$ are rather monotonic, with the $\kappa \nabla T$ heat transport near the wall gradually taken up by the increasing $T s v_n(x)$ contribution. $\delta \mu_n(x)$ is increasing as one moves away from the wall, but shows a rather peculiar non-monotonic behavior near the wall. The reason for this is due to the rapid increasing of local equilibrium density of quasiparticles within the length of several mean free paths towards the wall. Then the density deviation of quasiparticles to the local equilibrium value decreases and the quasichemical potential increases as one moves very close to the wall. Since this “half space” geometry carries less information than the “sandwich” case, the discussion of the sandwich case is as follows.

4.2 Sandwich Case

For the sandwich case the space is simply discretized with the help of the symmetry (2.50), resulting in a closed set of linear equations at the discrete x , and $-L/2 < x < 0$. Here another problem arises: at $x = 0$ all the equations

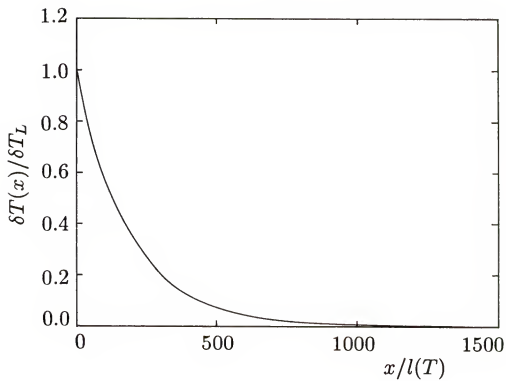


FIG. 3(a). Temperature profile of superfluid ${}^3\text{He-B}$ at $T = 0.85T_c$ in half infinite case. $l(T)$ is the mean free path.

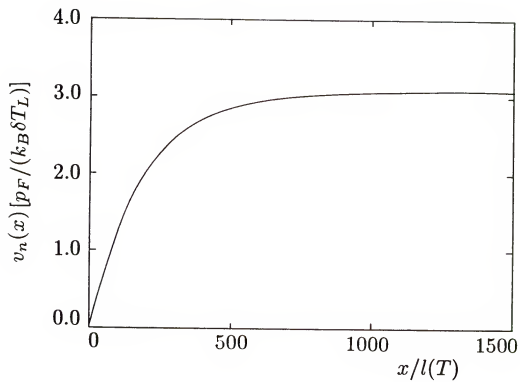


FIG. 3(b). Velocity profile of superfluid ${}^3\text{He-B}$ at $T = 0.85T_c$ in half infinite case. $l(T)$ is the mean free path.

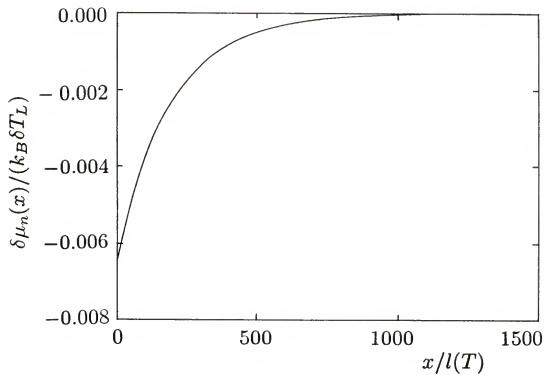


FIG. 3(c). Pseudo-chemical potential profile of ${}^3\text{He-B}$ at $T = 0.85T_c$ in half infinite case. $l(T)$ is the mean free path.

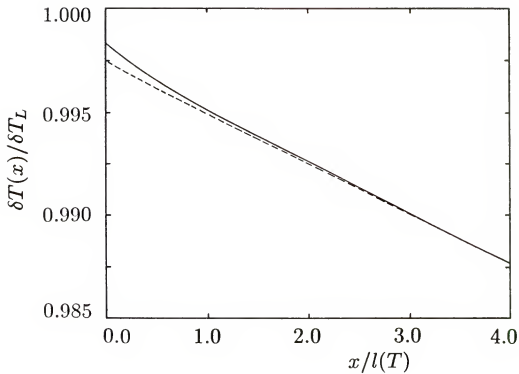


FIG. 4. Deviation of the temperature profile of the hydrodynamic approach (dashed line) to the numerical result (solid line) for ${}^3\text{He-B}$ at $T = 0.2T_c$ in half infinite case. $l(T)$ is the mean free path.

(2.45),(2.48),(2.49) are trivially satisfied when the symmetry relations (2.50) are used. However, if N discrete points are put on $x = -L/2$ to $x = 0$ then the $x = 0$ value for $v_n(x)$ is still necessary, and three more equations are needed. To resolve this “difficulty”, consider if the symmetry relations (2.50) are not used and the whole space $\frac{L}{2} \geq x \geq -\frac{L}{2}$ is discretized, then it can be seen from the equations (2.45,2.48,2.49) that (2.50) must be satisfied. Therefore when one is using (2.50) in (2.45,2.48,2.49), equation (2.50) represents a condition which should be kept, or else some information would be lost. While $\frac{dv_n(x)}{dx} = \frac{dv_n(-x)}{dx}$ has been put in, $\delta T(0) = 0$ and $\delta \mu_n(0) = 0$ are then the two missing equations. Hence it is necessary to add these equations by hand and to complete the coupled equations.

One may wonder that the above “difficulty” is inherent in the use of $\sum p_x v_{p_x} \delta f_p'' = c_a$ and $\sum E_p v_{p_x} \delta f_p'' = c_b$ as conservation equations, as for the half space the $x = \infty$ value has to be used to fix the constant c_a and c_b , and they are also responsible for the trivial equations for the sandwich at $x = 0$. Using $\sum p_x \delta f_p'' = 0$ and $\sum E_p \delta f_p'' = 0$, the momentum and energy conservation under collision, would solve both these problems. However, using these equations produces an even greater difficulty. For example in the sandwich case one would obtain

$$\begin{aligned}
0 = & -2K_0(0)v_n(x) - \frac{M_0(x + \frac{L}{2}) + M_0(-x + \frac{L}{2})}{T} (\delta T(-\frac{L}{2}) - \delta T_L) \\
& + \int_{-L/2}^{L/2} dx' \{ K_{-1}(|x - x'|)v_n(x') - [L_0(|x - x'|) \\
& - \frac{L_0(x + \frac{L}{2}) + L_0(-x + \frac{L}{2})}{2}] \frac{d\mu_n(x')}{dx'} - \frac{M_0(|x - x'|)}{T} \frac{dT(x')}{dx'} \}
\end{aligned} \tag{4.6}$$

One may easily verify that (4.6) is equivalent to (2.45) by simply taking the derivative of the latter, and using integration by parts.

To see the difficulty one tries to show the hydrodynamic limit from (4.6). Using the same argument as in Sec.3.2, one notices that the lowest order expansion of the $v_n(x')$ term under the integral is exactly canceled by $-2K_0v_n(x)$, the next order term in the expansion vanishes in the hydrodynamic regime, while the third order term survives and gives a term involving $\frac{d^2v_n}{dx^2}$, one would obtain

$$0 = -2K_2(0)\frac{d^2v_n(x)}{dx^2} + 2L_1(0)\frac{d\mu_n(x)}{dx} + \frac{2M_1(0)}{T}\frac{dT(x)}{dx} \quad (4.7)$$

which is just the derivative of (3.13) as one may expect. However, this shows that in a numerical calculation (i) the lowest and next order terms have to cancel so that no spurious extra term arises and (ii) the second derivatives are represented to sufficient accuracies to produce the hydrodynamic limit (4.7). This is rather non-trivial, and that is why we prefer rather special choice of deriving our integral equations.

In the discretization the intervals are always in the range of $h < \ell(T)$ so that the unknown variables ($\delta T(x)$ etc.) vary slowly from one point to the next at least in the hydrodynamic regime. The same procedures as those in the half space case can be used. In each interval one pulls the thermodynamic variables outside the integral and the integral of the kernel can be done exactly. Hence only kernels with subscripts one larger than those that appear explicitly in (2.45,2.48,2.49) are involved. One can check from their definition (2.28) that all these kernels are well defined and their momentum sums can be calculated without difficulty.

Fig.5 at $T/T_c = 0.5$, shows $\delta T(x)$, $v_n(x)$, $\delta\mu_n(x)$ for three values of $L/\ell(T)$, chosen for three different regimes as discussed in section 3.1. For $L/\ell(T) = 4 \times 10^3$, $L > \lambda(T) > \ell(T)$, it is apparent that an exponential decay of $\delta T(x)$ occurs at the wall. For $L/\ell(T) = 80$ ($\lambda(T) \sim 250\ell(T)$), $\lambda(T) > L(T) \gg \ell(T)$

and hydrodynamics applies. It follows from (3.29) and (3.30) that $\delta T(x)$ is approximately linear and $v_n(x)$ approximately quadratic in x . In this case the “s-q modes” near the two walls couple strongly with each other. In both these two cases the temperature jumps at the wall (and hence the conventional Kapitza resistances) are small compared with the temperature changes inside the fluid. Near (but not too near) to the walls, it is easy to check that the $-\kappa \nabla T$ term essentially carries all the heat flow.

Since for a superfluid, a uniform ∇T is not a solution to the hydrodynamic equations, this ∇T is gradually converted to the Tsv_n term (the s-q mode). Although the result that the temperature jump at the wall is small may be specific to our boundary condition (which allows a maximum heat transfer between the fluid and the wall), it does call for more careful theoretical and experimental treatments of Kapitza resistance of superfluid ^3He .

For the last case, $L/\ell(T) = 0.5$ one is in the Knudsen regime $L \ll \ell(T)$. Here the mean free path of the quasiparticles is actually larger than that of the size of the system, and quasiparticles are bouncing from one wall to the other, exchanging the energy. Nowhere does the hydrodynamics apply, and the $\delta T(x)$, $v_n(x)$, and $\delta\mu_n(x)$ should be understood as that defined from the local energy, momentum and number density.

Now the numerical solution to the kinetic equations for ^3He is obtained. By doing the numerical calculation at several values of $L(L \sim \lambda \gg \ell(T))$ it is possible to find the surface Onsager coefficients a , b and c .

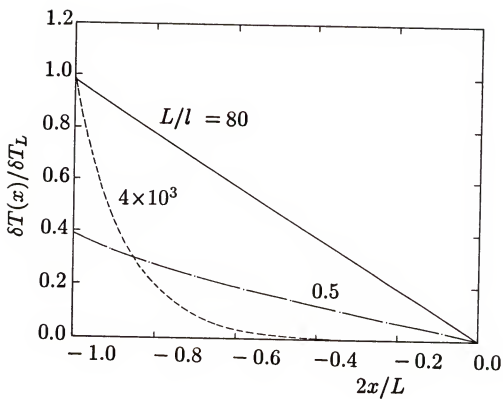


FIG. 5(a). Temperature profile of superfluid ${}^3\text{He-B}$ at $T = 0.5T_c$ in a slab of width L for three values of L/l (l is the mean free path).

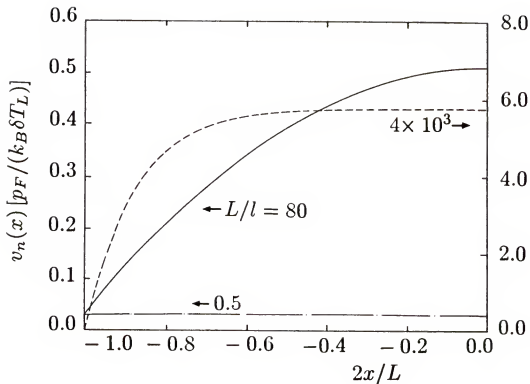


FIG. 5(b). Velocity profile of superfluid $^3\text{He-B}$ at $T = 0.5T_c$ in a slab of width L for three values of L/l (l is the mean free path).

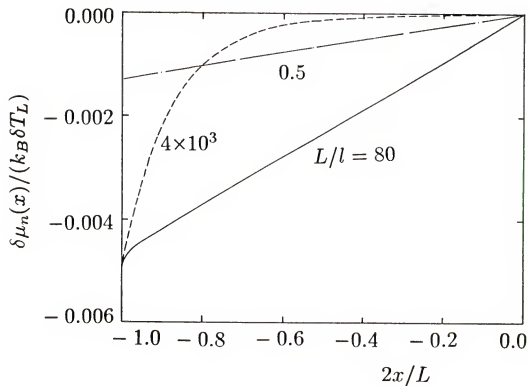


FIG. 5(c). Pseudo-chemical potential profile of ${}^3\text{He-B}$ at $T = 0.5T_c$ in a slab of width L for three values of L/l (l is the mean free path).

CHAPTER 5 MACROSCOPIC BOUNDARY CONDITION

5.1 Entropy Flow and Superfluid Flow

In normal fluid, all one needs is the value of the entropy flow f , which fixes the thermal gradient at the boundary, $f = -(\kappa/T)T'(0)$, and yields uniqueness of the solution to the hydrodynamic equations. In superfluids, however, there are two flow fields here, v_s and v_n , even in the hydrodynamic regime, the macroscopic boundary conditions for the case of thermal flow are more complex than previously thought. Two related aspects of this are

(i) That the entropy f in a superfluid is the sum of a convective and diffusive component $f = sv_n - (\kappa/T)\frac{dT}{dx}$ (s entropy density, κ thermal conductivity) and

(ii) That in the static limit, the temperature $T(x)$ and normal velocity $v_n(x)$ in the presence of a stationary entropy flow f vary according to (linearized) hydrodynamics^{71,72} as $T - T_\infty = T_s^- e^{x/\lambda} + T_s^+ e^{-x/\lambda}$ and $sv_n = \bar{\kappa}(T - T_\infty) + f$. Here λ is a characteristic length associate with counterflow, given by $\lambda^2 = \alpha\kappa/s^2T$, where $\alpha = \frac{4}{3}\eta - 2\zeta_1\rho + \zeta_2 + \zeta_3\rho^2$ is a combination of viscosity coefficients, ρ is the mass density, and $\bar{\kappa} = \kappa/T\lambda$. In this chapter all symbols denote values in hydrodynamic description.

Accordingly, the temperature profile across a solid wall shows a jump at the wall (within the Knudsen layer of thickness $\sim \ell$) followed by an exponential decay region of width λ (“ λ regime”). As we will show in chapter 7 $\lambda \simeq \ell$ for superfluid ^4He , but $\lambda \simeq (T_F/T)\ell \gg \ell$ for superfluid ^3He as we discussed in section 3.2.

Thus, for ${}^4\text{He}$ the λ regime can not be separated from the Knudsen regime and it is perfectly reasonable to introduce a single temperature jump as in the study of sound propagation in ${}^4\text{He}$ as suggested by Khalatnikov²⁴ to give the whole load of thermal transport to $v_n = f/s$ and neglect the dissipative terms. In the case of ${}^3\text{He}$, on the other hand, the question is how the entropy flow is divided up into the convective and diffusive parts and which fraction of the total temperature jump (and even its sign) is due to the exponentially varying parts (T_s^\pm). This is determined by the boundary conditions and has been calculated in chapter 2 and 4 for diffuse scattering of quasiparticles at the wall.

The general hydrodynamic boundary conditions derived by Grabinski and Liu relate the entropy flow f_0 and the superfluid mass flow j_s (in the rest frame of the normal fluid) at the boundary to the temperature jump ΔT and the normal fluid velocity gradient dv_n/dx , as given in (1.1-2)

(1.1-2) is a general boundary condition, essential to supplement the bulk (not necessary static) differential hydrodynamic equations in order to find a solution (the derivation of the Onsager relation, see Appendix C). In the rest frame of the interface, g may be eliminated, yielding

$$f_0 = a\Delta T + \frac{c\alpha}{\rho} \frac{dv_n}{dx} \quad (5.1)$$

$$j_s = c\Delta T + \frac{b\alpha}{\rho} \frac{dv_n}{dx} \quad (5.2)$$

Here for definiteness, consider a wall on the left and the superfluid on the right of the surface at which the above equation should be applied. ΔT is the temperature jump at the boundary, v_n is the normal fluid velocity, ρ is the number density, f_0 is the entropy flux density in the rest frame, α is combinations of shear viscosity η and second viscosities $\zeta_{1,2,3}$: $\alpha = \frac{4}{3}\eta -$

$2\zeta_1\rho + \zeta_2 + \zeta_3\rho^2$, a, b, c are the (surface) Onsager coefficients, with $a, b > 0$ and $ab \geq c^2$. The hydrodynamic formula for the various fluxes are $f_0 = \frac{s}{\rho}j_s - \kappa\frac{\nabla T}{T}$, $j_s = \rho_s(v_s - v_n)$. Here s is the entropy density, κ is the thermal conductivity, ρ_s is the superfluid number density, and the velocities are with respect to the laboratory frame.

Let us first ignore the cross coefficient c , then (5.1) is a relation between the heat flux and the temperature jump at the boundary, and is thus the usual Kapitza type of relation and (5.2) is a linear equation involving v_n and $\frac{dv_n}{dx}$ at the wall. This is the most general type of boundary condition for a quantity that obeys a second order differential equation in the bulk, and is analogous to the transverse flow case.^{18,19} The coefficient c represents the fact that the heat and normal fluid flow are coupled.

In ^4He , they combine to yield only one, the Kapitza resistance, for all conceivable experimental situations. Thus the boundary conditions reduce to those of Khalatnikov, supplemented by $T'(0) = 0$. In superfluid ^3He , all three Onsager coefficients remain independent and hence relevant to the interpretation of different experimental situations.

5.2 Onsager coefficients

The relation of Onsager coefficients a, b, c with the temperature jump at the wall and entropy flux for the half space case has been discussed in Ref.22. In the hydrodynamic regime

$$T(x) = T_s^+ e^{-x/\lambda} \tag{5.3}$$

$$f = sv_n - \frac{\kappa}{T} \frac{dT}{dx} \tag{5.4}$$

Substitute (5.3),(5.4) to (5.1),(5.2), noticing $\alpha = \frac{\lambda^2 s^2 T}{\kappa}$ as derived in section 3.2 (3.25) and $\bar{\kappa} = \frac{\kappa}{T\lambda}$, $f = const$, it can be obtained that

$$f = a\Delta T + c\sigma(-T_s^+) \quad (5.5)$$

$$-\rho v_n = c\Delta T + b\sigma(-T_s^+) \quad (5.6)$$

and then the entropy expression

$$-\frac{f}{\sigma} + \frac{\bar{\kappa}}{\sigma} T_s^+ = c\Delta T + b\sigma(-T_s^+) \quad (5.7)$$

here $\sigma = s/\rho$, and

$$\frac{\Delta T}{f} = \frac{b\sigma^2 + c\sigma + \bar{\kappa}}{(ab - c^2)\sigma^2 + \bar{\kappa}a} \quad (5.8)$$

$$\frac{T_s^+}{f} = \frac{a + c\sigma}{(ab - c^2)\sigma^2 + \bar{\kappa}a} \quad (5.9)$$

For the sandwich case, consider symmetry condition (2.50)

$$\delta T(x) = 2T_s^- \sinh \frac{x}{\lambda} \quad (5.10)$$

Substitute (5.10) to (5.1) and (5.2) then

$$f = a\Delta T + 2c\sigma T_s^- \sinh \frac{L}{2\lambda} \quad (5.11)$$

$$j_s = c\Delta T + 2b\sigma T_s^- \sinh \frac{L}{2\lambda} \quad (5.12)$$

with (5.4), (5.12) can be written as

$$c\Delta T + 2b\sigma T_s^- \sinh \frac{L}{2\lambda} = -\rho \left(\frac{f}{s} + \frac{\kappa}{T_s \lambda} 2T_s^- \cosh \frac{L}{2\lambda} \right) \quad (5.13)$$

thus

$$\frac{\Delta T}{f} = \left\{ 2\bar{\kappa} \cosh \frac{L}{2\lambda} + 2(b\sigma^2 + c\sigma) \sinh \frac{L}{2\lambda} \right\} / D \quad (5.14)$$

$$\frac{T_s^-}{f} = -(a + c\sigma) / D \quad (5.15)$$

here

$$D = 2\bar{\kappa}a\cosh\frac{L}{2\lambda} + 2(ab - c^2)\sigma^2\sinh\frac{L}{2\lambda} \quad (5.16)$$

and also

$$\begin{pmatrix} a & c\sigma 2\sinh\frac{L}{2\lambda} \\ c\sigma & b\sigma^2 2\sinh\frac{L}{2\lambda} + \bar{\kappa}2c\cosh\frac{L}{2\lambda} \end{pmatrix} \begin{pmatrix} \frac{\Delta T}{f} \\ \frac{T_r}{f} \end{pmatrix} = \begin{pmatrix} 1 \\ -1 \end{pmatrix} \quad (5.17)$$

This means that if the Onsager coefficients a, b, c are known, the temperature profile across the half space and also other quantities can be obtained. But in the macroscopic hydrodynamic description the Onsager coefficients a, b, c are phenomenological coefficients. To determine a, b, c one needs a microscopic theory. Based on the results of chapter 4, by fitting the numerical results in the limit $L/\ell \gg 1$ to the hydrodynamic limit calculated employing the boundary condition (5.1-2), we can determine the Onsager coefficients a, b, c .

For the half space case, noticing that we have two equations (5.8) and (5.9), one finds that it is impossible to determine all the three unknown quantities. For the sandwich case, from eq.(5.17), one has independent equations for different L . The obtained a, b, c values should satisfy all those equations including those in the half space case, i.e. (5.8-9).

In the hydrodynamic limit, if $\delta T(\pm\frac{L}{2}), v_n(\pm\frac{L}{2})$ denote the values of the temperature and velocity extrapolated to the walls, and ΔT denotes the extrapolated jump at the wall, i.e. $\Delta T = \delta T(\frac{L}{2}) - \delta T_R$, and $\delta T(\frac{L}{2}) - \delta T_R = \delta T_L - \delta T(-\frac{L}{2})$, then one may introduce the following dimensionless variables.

$$\tilde{f} = f \frac{PF}{s(T)k_B\delta T_L} \quad (5.18)$$

$$\Delta\tilde{T} = \frac{\Delta T}{\delta T_L} \quad (5.19)$$

$$\tilde{a} = a \frac{2T_F}{s(T)v_F} \quad (5.20)$$

$$\tilde{b} = b\sigma^2 \frac{2T_F}{s(T)v_F} \quad (5.21)$$

$$\tilde{c} = c\sigma \frac{2T_F}{s(T)v_F} \quad (5.22)$$

here, $\sigma = s/\rho$, $T_F = p_F v_F / 2k_B$. Substituting (5.18-5.22) and the relations

$$f = sv_n(-\frac{L}{2}) - \bar{\kappa}T_s^- 2\cosh\frac{L}{2\lambda} \quad (5.23)$$

$$T(-\frac{L}{2}) = -2T_s^- \sinh\frac{L}{2\lambda} \quad (5.24)$$

to (5.17) one finds

$$\tilde{a}\Delta\tilde{T} - \tilde{c}(1 - \Delta\tilde{T}) = \tilde{f} \quad (5.25)$$

$$\tilde{c}\Delta\tilde{T} - \tilde{b}(1 - \Delta\tilde{T}) = -\frac{p_F v_n(-\frac{L}{2})}{k_B \delta T_L} \quad (5.26)$$

The results for $\tilde{a}, \tilde{b}, \tilde{c}$ are shown in Fig.6. The quantity \tilde{a} is large and positive, whereas \tilde{b} and \tilde{c} are small, \tilde{b} is positive and \tilde{c} is negative. This leads to (i) the temperature jump at the wall being negligible compared to the amplitude $T_s^{+,-}$ of the exponential decay in the λ layer and (ii) the boundary condition at the wall being $f \simeq -\frac{\kappa}{T} \frac{dT}{dx}$.

With the a, b, c values and boundary condition (5.1-2), the hydrodynamic description of transport phenomena of ^3He becomes possible and transparent as mentioned in section 5.1. The significance of the Onsager coefficients will be discussed again in the next section and in chapter 6.

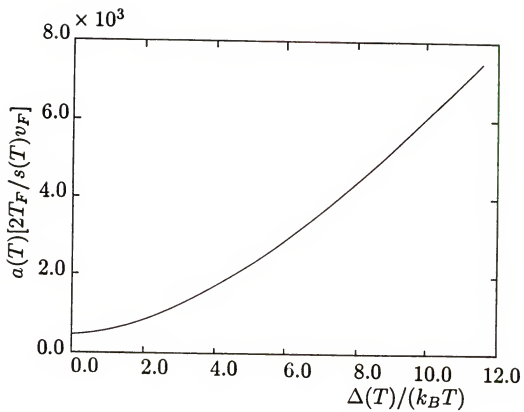


FIG. 6(a). Surface Onsager coefficients a as a function of temperature. Plotted are the normalized quantities $a(2T_F/sv_F)$ vs $\Delta(T)/T$.

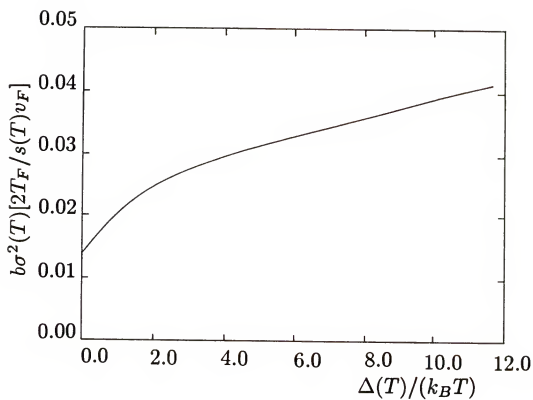


FIG. 6(b). Surface Onsager coefficients b as a function of temperature. Plotted are the normalized quantities $b\sigma^2(2T_F/sv_F)$ vs $\Delta(T)/T$.

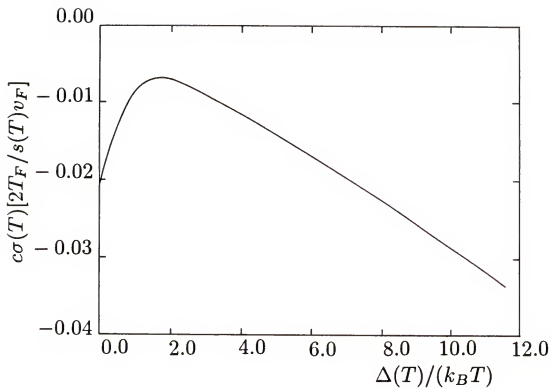


FIG. 6(c). Surface Onsager coefficients c as a function of temperature. Plotted are the normalized quantities $c\sigma(2T_F/sv_F)$ vs $\Delta(T)/T$.

5.3 Slip Length

As mentioned in section 5.1, the Onsager relation (5.1-2) involving v_n and $\frac{dv_n}{dx}$ at the wall is a general type of boundary condition. In this section we consider another method to describe the macroscopic boundary condition.

As a first correction to hydrodynamics one may introduce the concept of fluid slip, taking into account that the fluid velocity at the wall is not quite zero (in the frame of reference where the velocity of the wall is zero). The distance from the wall at which the fluid velocity extrapolates to zero is the so-called slip length ξ_λ . Notice that when the mean free path of thermal excitations is comparable to or even larger than the dimensions of the container, slip theory is no longer applicable in a strict sense (although it may still give reasonable results). In the latter case, the so-called Knudsen regime, one must resort to a microscopic description in terms of a distribution function for quasiparticles in momentum space.

Analogous to the transverse flow case,^{18,19} it is possible to define a similar concept of slip length relating the velocity gradient near the wall to the extrapolated velocity at the wall.

$$v_n(0) = \xi_\lambda \frac{dv_n}{dx} \quad (5.27)$$

This phenomenological slip boundary condition is only suitable for calculating corrections to the hydrodynamic description, i.e. for $L/\ell \gg 1$. The ξ_λ value can be obtained from numerical results directly, and it can also be derived from the a, b, c values and verified by comparison with that derived from numerical results.

1. Half space case. In the hydrodynamic description (3.27),

$$v'_n(0) = -\frac{1}{\lambda}(v_n(0) - v_n(\infty)) \quad (5.28)$$

and

$$\xi_\lambda = \frac{\lambda v_n(0)}{v_n(\infty) - v_n(0)} \quad (5.29)$$

here $v_n(\infty) = f/s$, substitute (5.6) to (5.29)

$$\xi_\lambda = \frac{\lambda(b\sigma^2 \frac{T^+}{f} - c\sigma \frac{\Delta T}{f})}{1 - (b\sigma^2 \frac{T^+}{f} - c\sigma \frac{\Delta T}{f})} \quad (5.30)$$

by using (5.8) and (5.9) it is obtained

$$\xi_\lambda = \frac{\lambda(ab\sigma^2 - c^2\sigma^2 - \bar{\kappa}c\sigma)}{\bar{\kappa}(a + c\sigma)} \quad (5.31)$$

from numerical calculation we know that $ab\sigma^2 \gg c\sigma(\bar{\kappa} + c\sigma)$ and $a \gg c\sigma$ then $\xi_\lambda \sim \lambda b\sigma^2/\bar{\kappa}$.

2. Sandwich case. From (3.30) it is obtained

$$v'_n \Big|_{x=-\frac{L}{2}} = -\frac{\kappa}{T\lambda} \frac{1}{s\lambda} (2T_s^-) \sinh \frac{L}{2\lambda} \quad (5.32)$$

then,

$$\xi_\lambda = \frac{v_n(-\frac{L}{2})}{v'_n(-\frac{L}{2})} \quad (5.33)$$

That is

$$\xi_\lambda = \lambda \frac{sv_n(-\frac{L}{2})}{\frac{\kappa}{T\lambda} (-2T_s^-) \sinh \frac{L}{2\lambda}} \quad (5.34)$$

Notice (5.26), i.e.

$$-sv_n(-\frac{L}{2}) = c\sigma\Delta T - b\sigma^2(\delta T_L - \Delta T) \quad (5.35)$$

(5.34) can be rewritten as

$$\xi_\lambda = \lambda \frac{b\sigma^2(\frac{\delta T_L}{f} - \frac{\Delta T}{f}) - c\sigma \frac{\Delta T}{f}}{\bar{\kappa}(-\frac{2T_s^-}{f}) \sinh \frac{L}{2\lambda}} \quad (5.36)$$

Notice $\delta T_L = -2T_s^- \sinh \frac{L}{2\lambda}$,

$$\xi_\lambda = \lambda \frac{b\sigma^2 \left(-\frac{2T_s^-}{f}\right) \sinh \frac{L}{2\lambda} - (b\sigma^2 + c\sigma) \frac{\Delta T}{f}}{\bar{\kappa} \left(-\frac{2T_s^-}{f}\right) \sinh \frac{L}{2\lambda}} \quad (5.37)$$

Substitue (5.14) and (5.15) to (5.37), then

$$\xi_\lambda = \lambda \left(\frac{b\sigma^2}{\bar{\kappa}} - \frac{b\sigma^2 + c\sigma}{a + c\sigma} \coth \frac{L}{2\lambda} - \frac{(b\sigma^2 + c\sigma)^2}{\bar{\kappa}(a + c\sigma)} \right) \quad (5.38)$$

$a \gg c\sigma$, $b\sigma^2$, for the case of $L/2\lambda$ not too small, i.e. in the hydrodynamic regime. $\xi_\lambda \sim \lambda b\sigma^2/\bar{\kappa}$. This is the same as that in the case of half space.

We should mention here that the Onsager relation and slip length are macroscopic description of the hydrodynamic boundary condition, and are not suitable to the Knudsen regime. One can see that in (5.38), if $L/2\lambda$ is too small, the ξ_λ is not correct, and even turns to be negative.

This slip length, in the light of the calculated a, b, c values, is essentially determined entirely by the b value. This is because $|\tilde{b}| \sim |\tilde{c}|$ and $|T_s^- \sinh \frac{L}{2\lambda}| \gg \delta T$, except for very small $L/2\lambda$, therefore the off-diagonal c terms can always be ignored there, and b defines the slip length. The slip length $\xi_\lambda \sim b\sigma^2\lambda/\kappa$ is small and of the order of the mean free path $\ell(T)$, except as $T \rightarrow T_c$ where it diverges as λ^2 . The behavior of ξ_λ is shown in Fig.7. Hence near the wall, if $L \gg \ell(T)$, the normal velocity is typically small ($\xi_\lambda = 0$ would mean $v_n = 0$ at the wall). The value of ξ_λ obtained by Onsager coefficients agree with that obtained by numerical results perfectly well.

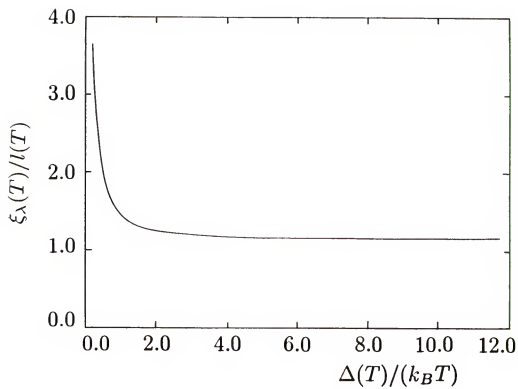


FIG. 7. The ratio of slip length $\xi_\lambda(T)$ to the mean free path $l(T)$ calculated from the half space geometry as a function of $\Delta(T)/(k_B T)$.

CHAPTER 6 BOUNDARY THERMAL RESISTANCES

6.1 Hydrodynamic Regime

It was demonstrated by Kapitza in 1941⁷³ that the flow of heat \dot{Q} from a solid body to liquid helium produces a temperature discontinuity ΔT at the interface. This phenomenon is now referred to as Kapitza resistance. The mechanism of heat transfer between classical fluid and solid is well established due to phonons as suggested by Khalatnikov.²⁴ The corresponding thermal resistance with one side replaced by a quantum fluid is still rather controversial, even when the quantum fluid is not in the superfluid state, even less is known for the superfluids (see for example, the review by Harrison⁷⁴).

The transfer of heat from a solid to the quasiparticles of ^3He is probably a complex process at the interface, energy may be transferred to (a) longitudinal zero sound (b) transverse zero sound (c) particle-hole excitations or (d) single-quasiparticle excitations. An extension of acoustic mismatch to ^3He at low temperature has been made by Bekarevich and Khalatnikov.⁷⁵ The direct transfer of energy from ^3He quasiparticles to paramagnetic atoms in a solid (CMN in particular) via magnetic coupling as suggested by Peshkov⁷⁶ and Wheatley,⁷⁷ was first investigated theoretically by Leggett and Vuorio⁷⁸ and later by Mills and Béal-Monod.⁷⁹

Considering the thermal resistance between electrons and phonons in a metal or between the spins and phonons in a paramagnetic salt in experiments, the problem of thermal transport may be even more complicated.⁷⁴

The present investigation will thus focus on the qualitatively new features of this counterflow induced heat exchange problem. To achieve this aim, we make the simplest possible assumption, namely that the ${}^3\text{He}$ system is modelled by a single relaxation time Landau-Boltzmann equation and a diffuse scattering mechanism at the boundaries. It is well known that in ${}^3\text{He}$ since the surface affects the magnitude of the gap parameter, via pair breaking,^{26,27} Andreev reflections^{80–82} will occur near the wall. This anomalous process will be neglected in the following calculation, as it is expected to be important only at rather low temperatures.

Basically, at low temperatures the excitations in liquid helium have wavelengths and mean free paths much larger than the size of the container, or in most experimental cases, the size of the finely divided particles or pores between the particles. Thus the hydrodynamic description for bulk liquid helium is not appropriate at low temperatures, and special consideration of the boundary thermal resistance for the Knudsen regime is necessary as we will show in section 6.2.

The boundary thermal resistance is defined as the temperature of the wall relative to the temperature of ${}^3\text{He}$ at infinite distance divided by the heat flux for half space case,

$$R_{Thalfspace} = \frac{\delta T_L - \delta T(\infty)}{\dot{Q}} \quad (6.1)$$

and is defined as the temperature difference between slab divided by the heat flux for the sandwich case,

$$R_{Tsandwich} = \frac{\delta T_L - \delta T_R}{\dot{Q}} \quad (6.2)$$

\dot{Q} here is the total energy flux (consider symmetry relation, $\delta T_R = -\delta T_L$).

The proper Kapitza resistance (for a review, see Ref.74) associated with the temperature discontinuity ΔT at the boundary is usually defined as $R_K = \Delta T/Tf$, where T is the temperature of ^3He at a reference point, f is the entropy flux. Since ΔT turns out to be small except in the Knudsen regime, R_K will, in general, be small.

In this chapter both the hydrodynamic regime and the Knudsen regime are considered, and the thermal resistances will be recalculated from the Onsager coefficients and compared with that obtained from numerical results.

In the hydrodynamic regime, the thermal resistance can be calculated by the temperature and velocity profile for both the halfspace and the sandwich cases.

1. Half space. The thermal resistance can be written as

$$R_T = \frac{\delta T_L}{Ts(T)v_n(\infty)} \quad (6.3)$$

entropy $s(T)$ is given in (3.12) and substitute into (6.3), it is obtained

$$R_T = \frac{\pi^2 \hbar^3 v_F}{k_B^3 T_c^2 p_F} / \left[\left(\frac{T}{T_c} \right)^2 \left\langle \left(\frac{\xi}{k_B T} \right)^2 \right\rangle \left(\frac{p_F v_n(\infty)}{k_B \delta T_L} \right) \right] \quad (6.4)$$

here

$$\left\langle \left(\frac{\xi}{k_B T} \right)^2 \right\rangle = \int_{-\infty}^{\infty} d\xi \frac{\partial f}{\partial E} \left(\frac{\xi}{k_B T} \right)^2 \quad (6.5)$$

The critical temperature T_c and energy gap of ^3He satisfy⁶⁶

$$\Delta_B = 1.76 k_B T \tanh \left[\frac{\pi}{1.76} \left(\frac{2 \Delta C}{3 C_N} \right)^{\frac{1}{2}} \left(\frac{T_c}{T} - 1 \right)^{\frac{1}{2}} \right] \quad (6.6)$$

as $T \rightarrow T_c$, $\Delta \rightarrow 0$, from (3.12) then

$$s(T) = \frac{3}{\pi^2} s(T_c) \left(\frac{T}{T_c} \right) \left\langle \left(\frac{\xi}{k_B T} \right)^2 \right\rangle \quad (6.7)$$

We can rewrite (6.4) as

$$R_T = \frac{(\frac{p_F v_F}{k_B T_c})^{\frac{\pi^2}{3}} / (s(T_c) v_F)}{(\frac{T}{T_c})^2 < (\frac{\xi}{k_B T})^2 > (\frac{p_F v_n(\infty)}{k_B \delta T_L})} \quad (6.8)$$

2. Sandwich case. In the sandwich case, the entropy flux f is given in (3.5), the thermal conductivity κ is given in (3.9) and λ is given in (3.25). It is convenient to calculate the entropy flux f at the middle of the slab ($x = 0$) for $L \gg \ell$, the hydrodynamic regime.

The temperature profile is given in (5.10) and

$$f = -s v_n(0) - \frac{\kappa}{T} \frac{dT}{dx} \Big|_{x=0} \quad (6.9)$$

then

$$f = -\frac{1}{\pi^2 \hbar^3} \frac{p_F^2 < \xi^2 >}{v_F T} v_n(0) - \frac{\frac{p_F^2 v_F}{3\pi^2 \hbar^3} < \tau \xi^2 > (-2T_s^-)}{T^2} \frac{1}{v_F \tau} \frac{1}{p_F v_F} \left(\frac{27 < (\xi/k_B T)^2 >}{\frac{9}{5} + \frac{< (\xi/E)^2 >}{< (\Delta/E)^2 >}} \right)^{\frac{1}{2}} \quad (6.10)$$

Substitute (6.10) to (6.8) the thermal resistance from (6.2) is

$$R_T = \frac{(\frac{p_F v_F}{k_B T_c})^{\frac{\pi^2}{3}} / (s(T_c) v_F (\frac{T}{T_c})^2 < (\frac{\xi}{k_B T})^2 >)}{\frac{p_F v_n(0)}{k_B \delta T_c} + \left(\frac{3 < (\xi/k_B T)^2 >}{\frac{9}{5} + \frac{< (\xi/E)^2 >}{< (\Delta/E)^2 >}} \right)^{\frac{1}{2}} \left(\frac{-2T_s^-}{\delta T_L} \right)} \quad (6.11)$$

$v_n(0)$ and T_s^- can be obtained by the hydrodynamic fitting of the numerical results of temperature and velocity profile. Other parameters can be calculated by simple integrations.

6.2 Knudsen Regime

In a usual experimental situation the width of the slab L is fixed. At temperature $T = T_c$, $L \gg \ell$. As the temperature decreases, the mean free path ℓ increases exponentially,^{66,67,83} approximately as

$$\ell(T) = \ell(T_c) e^{\Delta/k_B T} \quad (6.12)$$

here, $\Delta(T)$ is given in (6.6), so that the ^3He in the slab enters the Knudsen regime as the temperature is low enough, and a microscopic description is necessary. Recall the energy flux equation in chapter 2 (2.47) and the kernel relation of (2.29), resulting in the expression for the heat flux

$$\begin{aligned} \dot{Q} = 2\{ & \int_{-\frac{\ell}{2}}^0 dx' M_0(|x'|) v_n(x') \\ & - \int_{-\frac{\ell}{2}}^0 dx' \frac{P_1(|x'|)}{T} \frac{dT(x')}{dx'} - P_1\left(\frac{L}{2}\right) \frac{\delta T(-\frac{\ell}{2}) - \delta T_L}{T} \} \end{aligned} \quad (6.13)$$

Notice that $s = 2M_1(0)/T$ and $\kappa = 2P_2(0)/T$ from (3.9), (3.12) and (3.19), (3.22) in the case of $L \gg \ell$. Using the same method as in section 3.2, expand $v_n(x')$ and $dT(x')/dx'$ in Taylor series about $x' = 0$, then the hydrodynamic approach (6.9) can be repeated. The last term of the right side in (6.13) is a kind of boundary effect and influences the total heat transfer from the wall to the superfluid. Fig.8 shows the total resistance R_T as function of T_c/T for the half space and the sandwich in the case $L < \lambda(T)$ always. For the half space case the result is indistinguishable from a straight line with slope $\Delta(T=0)/T_c$, i.e. $R_T \propto \exp(\Delta(T=0)/T)$ over the whole temperature range. For the sandwich case, at high temperatures $\ell(T) < L < \lambda(T)$ the resistance drops as the temperature decreases, until $\ell(T) \sim L$ where hydrodynamics breaks down. In the low temperature Knudsen regime $L \leq \ell(T)$, R_T increases exponentially as T lows, $R_T \propto \exp(\Delta/k_B T)$.

6.3 Results From Onsager Coefficients

In the last chapter we have shown that the Onsager relation gives a correct boundary condition to describe the hydrodynamic picture of superfluids and

gives temperature and velocity profiles. In this section we will derive the thermal resistance from Onsager coefficients.

1. Half space case. The definition of thermal resistance is rewritten as

$$R_T = \frac{\delta T_L}{Tf} \quad (6.14)$$

here $\delta T_L = \Delta T + (-T_s^-)$, under the assumption that the wall is in the left side, superfluid ${}^3\text{He}$ is in the right side. Substitute the (5.8-9) to (6.14), then

$$R_T = \frac{1}{T} \frac{\bar{\kappa} + a + 2c\sigma + b\sigma^2}{\bar{\kappa}a + (ab - c^2)\sigma^2} \quad (6.15)$$

Notice the renormalized relations (5.18-22)

$$R_T s(T_c) v_F = \frac{s(T_c) v_F}{T} \frac{2T_F}{s(T) v_F} \frac{1}{\bar{a}} \frac{1 + (a + 2c\sigma + b\sigma^2)/\bar{\kappa}}{1 + (b - c^2/a)\sigma^2/\bar{\kappa}} \quad (6.16)$$

Substitute the relation (6.7-8) to (6.16) finally,

$$R_T s(T_c) v_F = \frac{\pi^2/3}{(\frac{k_B T_c}{p_F v_F})} \frac{1}{(\frac{T}{T_c})^2} \frac{1}{(\frac{\xi}{k_B T})^2} > \frac{1}{\bar{a}} \frac{1 + (a + 2c\sigma + b\sigma^2)/\bar{\kappa}}{1 + (b - c^2/a)\sigma^2/\bar{\kappa}} \quad (6.17)$$

In the Onsager relation (5.1-2) for ${}^3\text{He}$, $a \gg b\sigma^2, c\sigma, \kappa$. R_T in (6.15) can be expressed as

$$R_T = \frac{\lambda}{\kappa} \quad (6.18)$$

with high accuracy. Substitute $\lambda^{-2} = \frac{T s^2}{\kappa \alpha}$ in (6.18), it is obtained that $R_T = \frac{1}{s} (\alpha/\kappa T)^{\frac{1}{2}}$. The T dependence of R_T is seen to be dominated by the entropy density s , which leads to an exponentially growing thermal resistance at low T

$$R_T = \frac{1}{s} \left(\frac{\pi^3}{2} \right)^{\frac{1}{2}} [T_c / C_N(T_c)] (T \Delta)^{-\frac{1}{2}} (\alpha/\kappa T)^{\frac{1}{2}} e^{\frac{\Delta}{k_B T}} \quad (6.19)$$

where $C_N(T_c)$ is the specific heat in the normal state at T_c and $(\alpha/\kappa T)^{1/2} \sim T_F/T_c v_F$ is a T -dependent limiting value. Now the exponential dependence of R_T in half space obtained by numerical results can well be understood, and the result of (6.17) agrees exactly with the numerical calculation as it should be

2. Sandwich case. The thermal resistance is defined

$$R_T = \frac{2\delta T_L}{Tf} \quad (6.20)$$

here, $\delta T_L = \Delta T + (-2T_s^-)sinh\frac{L}{2\lambda}$. Substitute (5.14-15) to (6.20), it is obtained

$$R_T = \frac{2\bar{\kappa} + (a + b\sigma^2 + 2c\sigma)tanh\frac{L}{2\lambda}}{T\bar{\kappa}a + (ab - c^2)\sigma^2tanh\frac{L}{2\lambda}} \quad (6.21)$$

as discussed in the last section,

$$R_T = \frac{\pi^2/3}{\left(\frac{k_B T_c}{p_F v_F}\right)\left(\frac{T}{T_c}\right)^2} \frac{1}{\left(\frac{\xi}{k_B T}\right)^2} > \bar{a} \frac{2\bar{\kappa} + (a + b\sigma^2 + 2c\sigma)tanh\frac{L}{2\lambda}}{\bar{\kappa} + (ab - c^2)\sigma^2tanh\frac{L}{2\lambda}} \quad (6.22)$$

for the same reason that $a \gg b\sigma^2, c\sigma, \bar{\kappa}$, and with high accuracy

$$R_T = (2\lambda/\kappa)tanh\frac{L}{2\lambda} \quad (6.23)$$

In the limit of wide slabs, $L \gg \lambda$, $R_T = (2/s)(\alpha/\kappa T)$ as discussed in last section. In the intermediate regime defined by $\ell \ll L \ll \lambda$, the thermal resistance becomes proportional to L and inversely proportional to the thermal conductivity

$$R_T = L/\kappa \quad (6.24)$$

Since κ is approximately proportional to $1/T$ in the whole temperature range⁷⁰, then $R_T \propto T$ in this regime. In other words, the thermal resistance R_T is expected to decrease with decreasing temperature, untill the mean free path increases sufficiently to become comparable with L .

For $L \ll \ell$, in the Knudsen regime, the hydrodynamic description breaks down. In Fig.8, $\ln R_T$ is shown as a function of T_c/T for a slab of width $L = 10\ell(T_c)$. In the neighborhood of T_c , $R_T \propto T$, as discussed above. Below the crossover temperature $0.5T_c$ into the Knudsen regime, $R_T \propto exp(\Delta/k_B T)$. For the sandwich, at high temperatures where hydrodynamics applies, the

agreement of the thermal resistances from Onsager coefficients and from numerical results is so good that the difference ($< 10^{-4}$ in the log scale, i.e. percentage difference of less than 0.01%) can not be shown on the plot. At lower temperatures, i.e. the Knudsen regime, the difference increasing as the temperature lowers, reaching 0.18 ($\simeq 2\%$ difference) at the temperatures that is investigated. Notice that at the low temperatures (in the deep Knudsen regime) equation (6.21) gives a good approximation $R_T = 2/aT$, i.e. the boundary resistance is dominated by the temperature jumps ΔT , the internal temperature change only furnishes a small correction.

It is also interesting to discuss the proper Kapitza resistance associated with the temperature discontinuity ΔT at the boundary, which is usually defined as $R_K \equiv \frac{\Delta T}{T}$. Since ΔT turns out to be small except in the Knudsen regime, R_K will in general be small. In terms of the surface Onsager coefficients a, b, c one may express R_K as $R_K \simeq (aT)^{-1}$, using $a \gg b\sigma^2, c\sigma$.

Experimental data^{84,85} appear to be consistent with $R_T \propto \exp(\Delta/k_B T)$, although an accurate comparison is difficult due to the complexity of the geometries employed and the uncertainties in the determination of the boundary surface area. More data on the thermal boundary resistance for slabs of different thickness are needed in order to test the predictions of our theory in detail.

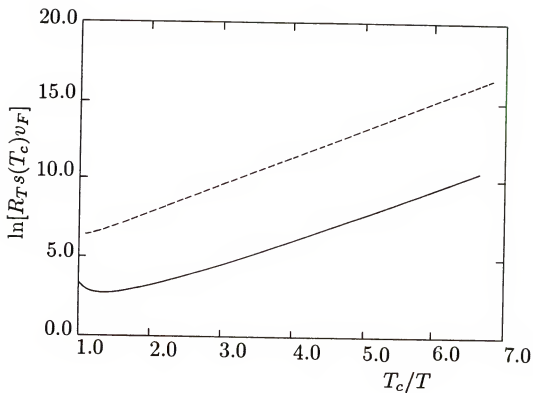


FIG. 8. Thermal resistance R_T across a slab of width $L = 10l(T_c)$ (solid line) and boundary resistance for a single surface bounding a half space volume of ${}^3\text{He-B}$ (broken line). Plotted is the logarithm of $R_{Ts}(T_c)v_F$ vs T_c/T .

CHAPTER 7 DISCUSSION OF ^4He CASE

7.1 Kinetic Equation for ^4He in Phonon Case

At $T = 2.18\text{K}$, ^4He undergoes a second order phase transition. At temperature below the phase transition point, liquid ^4He has a number of unusual properties, of which the most important is superfluidity. This phenomenon was discovered by Kapitza in 1937.⁸⁶ Liquid ^4He obeys the Bose statistics and is called Bose liquid. Based on the Landau quantum liquid concept,^{87,88} at temperature $T = 0$, the whole liquid flows without friction, but for $T \neq 0$, the excitations present in the liquid will be reflected at the wall and will transfer part of their momentum to the wall. Because of this, that part of the liquid that is carried along by the motion of the excitations will behave like a normal viscous liquid. Therefore in a superfluid two independent motions can take place simultaneously, superfluid motion with velocity v_s and normal part motion with velocity v_n .

From neutron scattering experiments⁸⁹ it has been possible to deduce the excitation spectrum of quasiparticles in ^4He . The part of the spectrum for small momentum k is the phonon regime and as p tends to zero the slope is the velocity of sound in the liquid, the part of the spectrum near the minimum is called the roton regime.⁸⁷ For phonon part the dispersion relation is $\epsilon = cp$, c is the sound velocity. For roton part the dispersion relation can be expressed as $\epsilon = \Delta + \frac{(p-p_0)^2}{2\mu}$, where Δ and p_0 are the energy and momentum coordinates of the minimum and μ is a constant related to the curvature at the minimum.

It is an important feature of the spectrum that only the low energy excitations are phonons. In the following discussion, we only consider the phonon part in the calculation.

The Boltzmann equation for the distribution function in momentum space of ^4He is of the same form as (2.12) and the boundary condition as (2.23), but the chemical potential from the set of hydrodynamic variables relevant for the time-independent flow is dropped, because the number of quasiparticles is not conserved in collision.

For the half space case the coupled momentum and energy conservation equations are

$$K_1(x)v_n(0) + \int_0^\infty dx' [K_1(|x-x'|) \frac{dv_n(x')}{dx'} - M_0(|x-x'|) \frac{\delta T(x')}{T}] = M_1(x) \frac{\delta T_L}{T} \quad (7.1)$$

$$2M_1(0)v_n(\infty) - \int_0^\infty dx' [M_0(|x-x'|)v_n(x') - P_1(|x-x'|) \frac{1}{T} \frac{dT(x')}{dx'}] = -P_1(x) \frac{\delta T(0) - \delta T_L}{T} \quad (7.2)$$

For the sandwich geometry, the momentum and energy conservation equations become

$$[K_1(\frac{L}{2} + x) - K_1(\frac{L}{2} - x)]v_n(-\frac{L}{2}) + \int_{-\frac{L}{2}}^{\frac{L}{2}} dx' K_1(|x-x'|) \frac{dv_n(x')}{dx'} - \int_{-\frac{L}{2}}^{\frac{L}{2}} dx' M_0(|x-x'|) \frac{\delta T(x')}{T} = [M_1(\frac{L}{2} + x) - M_1(\frac{L}{2} - x)] \frac{\delta T_L}{T} \quad (7.3)$$

$$\begin{aligned}
& [P_1(\frac{L}{2} + x) + P_1(\frac{L}{2} - x) - 2P_1(\frac{L}{2})] \frac{\delta T(-\frac{L}{2}) - \delta T_L}{T} \\
& + \int_{-\frac{L}{2}}^{\frac{L}{2}} dx' [P_1(|x - x'|) - P_1(|x'|)] \frac{dT(x')}{T dx'} \\
& - \int_{-\frac{L}{2}}^{\frac{L}{2}} dx' [M_0(|x - x'|) - M_0(|x'|)] v_n(x') = 0
\end{aligned} \tag{7.4}$$

The kernels $K_n(x)$, $M_n(x)$ and $P_n(x)$ are defined as in (2.28). In the linear phonon regime, the energy spectrum $\epsilon = cp$, where c is the sound velocity. The mean free path ℓ is assumed to be p independent for simplicity. The numerical results of temperature and the velocity profiles are shown in Fig.9.

Notice that in ${}^4\text{He}$ case, the thermal characteristic length λ is comparable to the mean free path. This is in contrast to a superfluid Fermi system, where the coupling of flow to the heat bath is weak, such that the healing length over which the temperature change relaxes become very long compared to the mean free path. Thus for ${}^4\text{He}$, the λ region can not be separated from the Knudsen regime and it is perfectly reasonable to introduce a single temperature jump at the wall as done usually.²⁴

7.2 Bounds for the Ratio $v_n(\infty)/\delta T_L$

With a very reasonable assumption, one can in fact obtain bounds for the ratio $v_n(\infty)/\delta T_L$ as follows, using

$$v_n(0) = v_n(\infty) - \int_0^\infty dx' \frac{dv_n(x')}{dx'} \tag{7.5}$$

$$\delta T(0) = \delta T(\infty) - \int_0^\infty dx' \frac{dT(x')}{dx'} \tag{7.6}$$

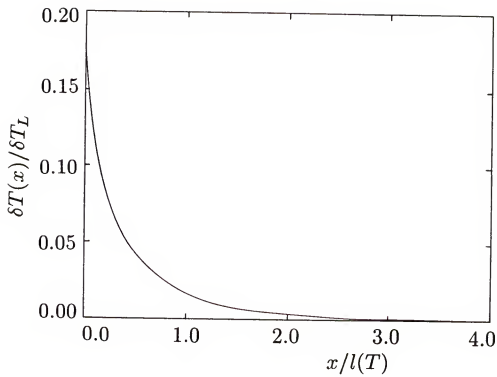


FIG. 9(a). Temperature profile of superfluid ^4He for phonon regime.

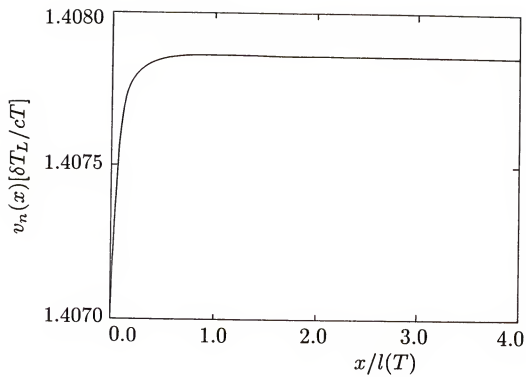


FIG. 9(b). Normal velocity profile of superfluid ^4He for phonon regime.

One may rewrite the equations analogous to (2.33) and (2.36) as

$$\begin{aligned}
& K_1(x)v_n(\infty) + M_1(x)\frac{\delta T(\infty)}{T} \\
& + \int_0^\infty dx' \left\{ \frac{dv_n(x')}{dx'} [K_1(|x-x'|) - K_1(x)] \right. \\
& \left. - M_0(|x-x'|)\frac{1}{T}[\delta T(x') - \delta T(\infty)] \right\} = M_1(x)\frac{\delta T_L}{T}
\end{aligned} \tag{7.7}$$

and

$$\begin{aligned}
& M_1(x)v_n(\infty) + P_1(x)\frac{\delta T(\infty)}{T} + \int_0^\infty dx' \left\{ \frac{1}{T}\frac{dT}{dx'} [P_1(|x-x'|) - P_1(x)] \right. \\
& \left. - M_0(|x-x'|)[v_n(x') - v_n(\infty)] \right\} = -2M_1(0)v_n(\infty) + \frac{P_1(x)\delta T_L}{T}
\end{aligned} \tag{7.8}$$

Assuming a monotonical dependence of $v_n(x)$ and $\delta T(x)$ and using $K_1(x) < K_1(0)$, $P_1(x) < P_1(0)$, $M_0(x) > 0$, it follows by putting $x = 0$ and noticing that $\delta T(\infty) = 0$ in (7.7) and (7.8), that

$$K_1(0)v_n(\infty) - M_1(0)\frac{\delta T_L}{T} \geq 0 \tag{7.9}$$

$$M_1(0)v_n(\infty) - P_1(0)\frac{\delta T_L}{T} \leq 0 \tag{7.10}$$

then we get

$$\frac{M_1(0)}{K_1(0)} \leq \left| \frac{v_n(\infty)}{\delta T_L/T} \right| \leq \frac{P_1(0)}{M_1(0)} \tag{7.11}$$

Both the left and right sides define weighted averages of the quasiparticle velocities, depending on the energy spectrum. For a phonon system with linear energy spectrum, the bounds can be evaluated from the kernel integrals (2.28) and finally,

$$\frac{4}{3} \leq \left| \frac{v_n(\infty)/c}{\delta T_L/T} \right| \leq \frac{3}{2} \tag{7.12}$$

These are rigorous bounds for the ratio $v_n(\infty)/\delta T_L$. The numerical result shows that this ratio equals 1.41, which is within the above bounds.

As mentioned in the last section there is no possibility to distinguish the hydrodynamic regime from the Knudsen regime, since the thermal characteristic length λ is comparable to the mean free path. If the hydrodynamic description is still used in the calculation of the ^4He case, it can be shown that the hydrodynamic prediction is beyond the bounds. Using the hydrodynamic description of $\delta T(x)$ from (3.26)

$$\delta T(x) = \delta T(0)e^{-x/\lambda} \quad (7.13)$$

and the energy flux conservation (3.5), then

$$v_n(x) = v_n(\infty) - \frac{\kappa}{sT\lambda}\delta T(0)e^{-x/\lambda} \quad (7.14)$$

where κ is the thermal conductivity, s is the entropy and λ is given by the expression $\lambda^{-2} = Ts^2/\kappa\alpha$ as before.

If the conventional boundary conditions $v_n(0) = 0$, $T(0) = T_L$ for the hydrodynamics are used (assuming a negligible temperature jump at the surface), the ratio $|\frac{v_n(\infty)/c}{\delta T_L/T}|$ would be $(5/3)^{\frac{1}{2}}$, which is beyond the rigorous bounds (7.12). The thermal decay length can be obtained from (7.7) and (7.8) with the same procedure as in the discussion of the ^3He case.

$$K_2(0)\frac{dv_n}{dx} - \frac{M_1(0)}{T}\delta T = 0 \quad (7.15)$$

$$\frac{P_2(0)}{T}\frac{dv_n}{dx} - M_1(0)v_n(x) = \text{const} \quad (7.16)$$

then

$$\frac{d^2T}{dx^2} - \frac{M_1^2(0)}{P_2(0)K_2(0)}\delta T = 0 \quad (7.17)$$

and

$$\lambda^{-2} = \frac{M_1^2(0)}{P_2(0)K_2(0)} \quad (7.18)$$

Substitute the kernel expressions to $M_1(0)$, $P_2(0)$ and $K_2(0)$, then it is easy to obtain that $\lambda = (3/5)^{\frac{1}{2}}\ell$, which is of the order of the mean free path. This

fact means that the hydrodynamic equations are not suitable to describe the temperature variation near the wall, and moreover, that variation should rather be incorporated in an effective boundary. Thus, instead of the three Onsager coefficients, they may be combined to yield only one, the boundary thermal resistance,

$$R_T = \frac{\delta T_L}{Tsv_n(\infty)} \quad (7.19)$$

and this value is 0.68/sc from the numerical results.

CHAPTER 8 FEMTOSECOND RELAXATION IN BULK GaAs

8.1 Band Structure

For many applications there is a need to know the band structure in a substantial part of the Brillouin zone. The bottom of the conduction band in GaAs type of semiconductors is degenerate. The valence band consists of two fold-degenerate subbands of heavy and light holes. Below the subbands of heavy and light holes, lies the so called spin split-off subband.^{90,91} The main features of the band structure in cubic semiconductors are summarized in table 2.2 in Ref.92.

The important features of the band structure of GaAs are the satellite minima at the L points separated from the Γ valley minimum by an energy $\Delta \sim 0.3eV$. The spherical Γ valley has a mass of $0.067m_e$. The L valleys are ellipsoidal, and the masses are not known well, although the density-of-states mass in the L valley has been estimated^{93,94} to about $m_L^* \sim 0.2m_e - 0.5m_e$.

The band structure for bulk GaAs⁴⁰ is shown in Fig.10. The excitations in the conduction and valence bands from the allowed optical transitions for a $2eV$ laser are shown by open circles.

In bulk GaAs only three $2eV$ transitions are possible, one each from the heavy, light and spin-split-off hole bands. There are only three narrow distinct optical coupled regions (OCR) in bulk GaAs on the order of the laser pulse width ($35meV$). The OCR are the regions in \vec{k} spsce in the conduction and valence bands for which optical transitions are possible. The two OCR's in

the conduction bands resulting from the light and heavy holes lie above the threshold for transfer into the L valleys, and the highest energy electrons from the heavy hole band transition are capable of scattering into the X valley.

We start the calculation with the initial distribution of three energy peaks centered at 0.11, 0.39 and 0.46eV, corresponding to transitions from the spin-split-off, light hole, heavy hole bands respectively as shown in Fig.11(a), the solid line. The initial peak shape is determined by the experimental lineshape of the laser and has a full width at half maximum of 40meV. The height of each peak is determined by the joint density of states for the transition and the intensity of the laser pulse. At high excitation intensities, saturation effects tend to equalize differences in transition strengths. There is little difference in the heavy and light hole transitions because away from the band edge, where this transition take place, band warping causes the two bands to have approximately the same effective masses.

8.2 Scattering Mechanisms

The scattering mechanisms considered are polar optical phonon (POP), intervalley deformation potential, acoustic phonon, ionized impurity, plasmon, electron-hole and electron-electron interactions. Approximations made in the scattering rate calculations are described below. We will focus on the polar optical phonon scattering and intervalley deformation potential scattering and neglect other scattering mechanisms.

The optical phonon scattering rate included assumes an equilibrium phonon population and is unscreened. For subpicosecond experiments the use of an

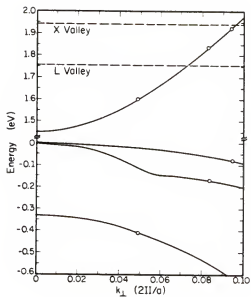


FIG. 10. The band structure of bulk GaAs from Ref. 96. The excitations in the conduction and valence bands from the allowed optical transition from a 2eV laser are shown by open circles.

equilibrium phonon population is a good approximation, since on a femtosecond time scale at room temperature relatively few phonons have been emitted, and a nonequilibrium phonon population can not be established. Intervalley phonon scattering is calculated using a deformation potential constant of 10^9 eV/cm as determined by Littlejohn et al.⁹⁵ for bulk GaAs. Because of higher effective masses and collisional broadening, the Γ and L valleys are assumed to have three dimensional density of states.

Acoustic phonon scattering is treated only in the elastic and intrasubband approximation. This is a reasonable assumption at room temperature since the acoustic scattering rate is small in GaAs and the energy exchanged in an acoustic phonon collision is much smaller than in a POP scattering. Thus, change in the electron distribution function due to acoustic phonon scattering is insignificant and is neglected in this calculation.

Electron-hole scattering is considered in the same manner as ionized impurity scattering because of the large effective mass ratio between electrons and holes in GaAs.⁹⁶ The effect of the holes on the relaxation rate is therefore lumped together with the effect of the impurities. This method treats electron-hole scattering as elastic, which is also supported by calculations of the energy loss rate of electrons to holes in bulk GaAs.⁹⁷ Electron-electron scattering in or with satellite-valley electrons is nearly elastic since the mass of the satellite valleys is much greater than the Γ valley mass. These types of elastic scattering should not influence the energy loss on a femtosecond time scale and are also neglected.

Plasmon scattering is not included in our calculation, although it is more important in two dimensions than in three dimensions because the plasmon frequency goes to zero with wave vector in two dimensions, making it possible to

emit plasmons at a much lower energy. For the highly nonequilibrium electron distributions found in $2eV$ photoexcitation experiments in undoped materials, after initial photoexcitation, there are few low energy electrons within the Γ valley. The nature of the plasmon mode for a highly nonequilibrium electron distribution, which can not be described by an effective electron temperature, is then unclear without a detailed many body calculation which goes beyond the scope of the present investigation.

The dynamics of the system is modelled with parabolic Γ and L valleys and a coupled set of Boltzmann equations one for the Γ valley and one for the L valley. A general set of Boltzmann equations for a nondegenerate system with two coupled valleys is

$$\begin{aligned} \frac{\partial f_{\Gamma}}{\partial t} = & - \sum_{k'} (W_{k,k'}^{\Gamma\Gamma} f_{\Gamma}(\epsilon_k) - W_{k',k}^{\Gamma\Gamma} f_{\Gamma}(\epsilon_{k'})) \\ & - \sum_{k'} (W_{k,k'}^{\Gamma L} f_{\Gamma}(\epsilon_k) - W_{k',k}^{L\Gamma} f_{L}(\epsilon_{k'})) \end{aligned} \quad (8.1)$$

$$\begin{aligned} \frac{\partial f_L}{\partial t} = & - \sum_{k'} (W_{k,k'}^{LL} f_L(\epsilon_k) - W_{k',k}^{LL} f_L(\epsilon_{k'})) \\ & - \sum_{k'} (W_{k,k'}^{L\Gamma} f_L(\epsilon_k) - W_{k',k}^{\Gamma L} f_{\Gamma}(\epsilon_{k'})) \end{aligned} \quad (8.2)$$

where f_{Γ} is the distribution function on the Γ valley and f_L is the distribution function in the L valley. The W is the transition rate which scatter from states on the left to states on the right, for example, $W_{k,k'}^{\Gamma L}$ is the transition rate for scattering from a state in the L valley with momentum k' to a state in the Γ valley with momentum k . The $W_{k,k'}^{\Gamma\Gamma}$ and $W_{k,k'}^{LL}$ are the polar optical phonon scattering rates.⁹⁸

$$W_{k,k'}^{\Gamma\Gamma} = \frac{2\pi}{\hbar} \left\{ \frac{2\pi e^2 \hbar \omega_{op}}{V_0 q^2 \epsilon} \left(\frac{1}{\epsilon_0} - \frac{1}{\epsilon_{\infty}} \right) \left(N_{op} + \frac{1}{2} \pm \frac{1}{2} \right) \right\} \delta(\epsilon(k') - \epsilon(k) \pm \hbar \omega_{op}) \quad (8.3)$$

$W_{k,k'}^{\Gamma L}$ and $W_{k',k}^{\Gamma L}$ are the intervalley optical deformation potential scattering rates¹⁰⁵

$$W_{k,k'}^{\Gamma L} = \frac{2\pi}{\hbar} \left\{ \frac{\hbar^2 D_{jk}^2 \gamma}{2V_0 \rho_0 \hbar \omega_0} \left(N_1 + \frac{1}{2} \pm \frac{1}{2} \right) \right\} \delta(\epsilon(k') - \epsilon(k) + \Delta \pm \hbar \omega_0) \quad (8.4)$$

where $N_{op} = [\exp(\hbar \omega_{op}/k_B T) - 1]^{-1}$, $N_1 = [\exp(\hbar \omega_0/k_B T) - 1]^{-1}$, $\vec{q} = \vec{k} - \vec{k}'$, and the values used for the material constants are $\epsilon_\infty = 10.92$, $\epsilon_0 = 12.9$, $\epsilon = 2.3$, the optical phonon energy $\hbar \omega_0 = 36 \text{ meV}$, the gap between the minimum of Γ and L valleys $\Delta_{L\Gamma} = 300 \text{ meV}$. The coupling constant $D_{jk} = 10 \times 10^8 \text{ eV/cm}$, the density of GaAs $\rho_0 = 5.36 \text{ g/cm}^3$ and γ is the number of final equivalent valleys.

8.3 Detailed Balance

The collision integrals in the coupled equations (8.1-2) must vanish when evaluated for the equilibrium Maxwellian distribution, otherwise the system can never reach equilibrium

$$\frac{\partial f_{\Gamma,eq}}{\partial t} \Big|_{coll} = \frac{\partial f_{L,eq}}{\partial t} \Big|_{coll} = 0 \quad (8.5)$$

Usually it is assumed that detailed balance holds. This means that

$$W_{k,k'}^{\Gamma\Gamma} f_{\Gamma,eq}(\epsilon_k) = W_{k',k}^{\Gamma\Gamma} f_{\Gamma,eq}(\epsilon_{k'}) \quad (8.6)$$

$$W_{k,k'}^{LL} f_{L,eq}(\epsilon_k) = W_{k',k}^{LL} f_{L,eq}(\epsilon_{k'}) \quad (8.7)$$

$$W_{k,k'}^{\Gamma L} f_{\Gamma,eq}(\epsilon_k) = W_{k',k}^{L\Gamma} f_{L,eq}(\epsilon_{k'}) \quad (8.8)$$

i.e. in equilibrium, all the individual scattering processes balance each other pairwise.⁹⁹ This assumption holds in equilibrium provided that the transition rates are given by the golden rule. Actually, out of equilibrium, detailed balance need not hold but one usually assumes that the scattering rates are not affected

by the external field. Clearly, this assumption of detailed balance is more restrictive than need be and there may be cases in which it is not valid. We shall use the assumption in the calculation, being aware that less restrictive models may apply.

With the assumption of detailed balance it is obvious that the total number of particles in both valleys is conserved in the collision processes

$$\sum_k \left(\frac{\partial f_\Gamma}{\partial t} \Big|_{coll} + \frac{\partial f_L}{\partial t} \Big|_{coll} \right) = 0 \quad (8.9)$$

The Maxwellian distribution functions $f_{\Gamma,eq}(\epsilon_k)$, $f_{L,eq}(\epsilon_k)$ in eq.(8.5) are proportional to $\exp[-(\epsilon_k - \mu_\Gamma)/k_B T]$ and $\exp[-(\epsilon_k - \mu_L)/k_B T]$ with the mass of the respective valleys. The chemical potentials characterizing the two local equilibrium functions are assumed to be equal. $\mu_\Gamma = \mu_L$, thus

$$\frac{f_{\Gamma,eq}(\epsilon_k)}{f_{L,eq}(\epsilon_{k'})} = \exp[(\epsilon_{k'} - \epsilon_k)/k_B T] \quad (8.10)$$

Of course similar relations hold for equilibrium distribution functions in the same valley.

CHAPTER 9 SOLUTION OF BOLTZMANN EQUATIONS

9.1 Coupled Boltzmann Equations

In the case of polar optical phonon scattering, to characterize the strength of the interaction one usually introduces the dimensionless Fröhlich coupling constant α_p defined by

$$\alpha_p = \frac{\epsilon^2}{\hbar\epsilon} \left(\frac{m}{2k_B\theta_{op}} \right)^{\frac{1}{2}} \left(\frac{1}{\epsilon_\infty} - \frac{1}{\epsilon_0} \right) \quad (9.1)$$

In general, if $\alpha_p < 1$ the electron-phonon coupling is considered weak, if $\alpha_p \simeq 5$ intermediate, and if $\alpha_p \geq 10$ strong.⁹² The α_p for the Γ valley in GaAs is about 5. The electrostatic nature of the interaction is such that the forward scattering is favoured so that this mechanism is strongly anisotropic. The treatment of this scattering is again simplified by the constancy of the phonon energy in the transition. At high electron energy, the total scattering rate for polar optical scattering decreases with increasing energy due to the electrostatic nature of interaction.¹⁰⁰

In the intervalley scattering, the phonon wavevector q involved in the transition is very close to the distance in the Brillouin zone between the minima of the initial and final valleys. Given these two valleys, q is almost constant, and therefore for a given branch of phonons, also the energy involved in the transition is approximately constant.⁹²

The coupled Boltzmann equations (8.1) and (8.2) can be expressed as

$$\begin{aligned} \frac{\partial f_{\Gamma}}{\partial t} = & \int_0^{\infty} d\epsilon_{k'} [S_{\Gamma,\Gamma}(\epsilon_k, \epsilon_{k'}) (f_{\Gamma}(\epsilon_k) - \frac{f_{\Gamma,eq}(\epsilon_k)}{f_{\Gamma,eq}(\epsilon_{k'})} f_{\Gamma}(\epsilon_{k'})) \\ & + S_{L,\Gamma}(\epsilon_k, \epsilon_{k'}) (f_{\Gamma}(\epsilon_k) - \frac{f_{L,eq}(\epsilon_k)}{f_{L,eq}(\epsilon_{k'})} f_L(\epsilon_{k'}))] \end{aligned} \quad (9.2)$$

$$\begin{aligned} \frac{\partial f_L}{\partial t} = & \int_0^{\infty} d\epsilon_{k'} [S_{L,L}(\epsilon_k, \epsilon_{k'}) (f_L(\epsilon_k) - \frac{f_{L,eq}(\epsilon_k)}{f_{L,eq}(\epsilon_{k'})} f_L(\epsilon_{k'})) \\ & + S_{\Gamma,L}(\epsilon_k, \epsilon_{k'}) (f_L(\epsilon_k) - \frac{f_{L,eq}(\epsilon_k)}{f_{\Gamma,eq}(\epsilon_{k'})} f_{\Gamma}(\epsilon_{k'}))] \end{aligned} \quad (9.3)$$

with

$$\begin{aligned} S_{\Gamma,\Gamma}(\epsilon_k, \epsilon_{k'}) = & M(\epsilon_k, \epsilon_{k'}) N_{op} \delta(\epsilon_{k'} - \epsilon_k - \hbar\omega_{op}) \\ & + M(\epsilon_k, \epsilon_{k'}) (N_{op} + 1) \delta(\epsilon_{k'} - \epsilon_k + \hbar\omega_{op}) \end{aligned} \quad (9.4)$$

$$\begin{aligned} S_{L,\Gamma}(\epsilon_k, \epsilon_{k'}) = & L(\epsilon_k, \epsilon_{k'}) N_1 \delta(\epsilon_{k'} - \epsilon_k - \hbar\omega_0 + \Delta) \\ & + L(\epsilon_k, \epsilon_{k'}) (N_1 + 1) \delta(\epsilon_{k'} - \epsilon_k + \hbar\omega_0 + \Delta) \end{aligned} \quad (9.5)$$

$$\begin{aligned} S_{L,L}(\epsilon_k, \epsilon_{k'}) = & K(\epsilon_k, \epsilon_{k'}) N_{op} \delta(\epsilon_{k'} - \epsilon_k - \hbar\omega_{op}) \\ & + K(\epsilon_k, \epsilon_{k'}) (N_{op} + 1) \delta(\epsilon_{k'} - \epsilon_k + \hbar\omega_{op}) \end{aligned} \quad (9.6)$$

$$\begin{aligned} S_{\Gamma,L}(\epsilon_k, \epsilon_{k'}) = & P(\epsilon_k, \epsilon_{k'}) N_1 \delta(\epsilon_{k'} - \epsilon_k - \hbar\omega_0 - \Delta) \\ & + P(\epsilon_k, \epsilon_{k'}) (N_1 + 1) \delta(\epsilon_{k'} - \epsilon_k + \hbar\omega_0 - \Delta) \end{aligned} \quad (9.7)$$

and the kernel integrals

$$M(\epsilon_k, \epsilon_{k'}) = -2\pi \int_0^{\pi} d\theta \sin\theta \left(\frac{2^{\frac{1}{2}} m_{\Gamma}^{*\frac{3}{2}}}{\hbar^3} \right) \frac{2\pi}{\hbar} \left\{ \frac{2\pi e^2 \hbar\omega_{op}}{V_0 \varepsilon q_{\Gamma}^2} \left(\frac{1}{\varepsilon_{\infty}} - \frac{1}{\varepsilon_0} \right) \right\} \epsilon_{k'}^{\frac{1}{2}} \quad (9.8)$$

$$L(\epsilon_k, \epsilon_{k'}) = -4\pi \left(\frac{2^{\frac{1}{2}} m_L^{*\frac{3}{2}}}{\hbar^3} \right) \frac{2\pi}{\hbar} \left\{ \frac{\hbar^2 D_{jk}^2 \gamma}{2V_0 \rho_0 \hbar\omega_0} \right\} \epsilon_{k'}^{\frac{1}{2}} \quad (9.9)$$

$$K(\epsilon_k, \epsilon_{k'}) = -2\pi \int_0^{\pi} d\theta \sin\theta \left(\frac{2^{\frac{1}{2}} m_L^{*\frac{3}{2}}}{\hbar^3} \right) \frac{2\pi}{\hbar} \left\{ \frac{2\pi e^2 \hbar\omega_{op}}{V_0 \varepsilon q_L^2} \left(\frac{1}{\varepsilon_{\infty}} - \frac{1}{\varepsilon_0} \right) \right\} \epsilon_{k'}^{\frac{1}{2}} \quad (9.10)$$

$$P(\epsilon_k, \epsilon_{k'}) = -4\pi \left(\frac{2^{\frac{1}{2}} m_{\Gamma}^{*\frac{3}{2}}}{\hbar^3} \right) \frac{2\pi}{\hbar} \left\{ \frac{\hbar^2 D_{jk}^2}{2V_0 \rho_0 \hbar\omega_0} \right\} \epsilon_{k'}^{\frac{1}{2}} \quad (9.11)$$

here q_Γ and q_L are defined as

$$q_\Gamma^2 = \frac{2m_\Gamma^*}{\hbar^2}(\epsilon_k - \epsilon_{k'})^2 \quad (9.12)$$

$$q_L^2 = \frac{2m_L^*}{\hbar^2}(\epsilon_k - \epsilon_{k'})^2 \quad (9.13)$$

The coupled rate equations (9.2) and (9.3) are related to the nonstationary processes and can be solved by matrix method as we will show in the next section.

9.2 Matrix Method Solution

The initial distribution of linear excited electrons is in an energy range about $0 - 520\text{meV}$ in Γ valley, as shown in Fig11(a), the solid line. In the relaxation process high energy electrons may transfer from Γ valley to L valley by absorption or emission of phonons. Recent Monte Carlo simulation results³⁹ show that $\Gamma - L$ scattering dominates the shift of electrons out of the heavy hole OCR. For the L valley the electrons transfer from the Γ valley located mainly at the bottom of the valley. Hence it is possible to cut the infinite up limit of integrations in (9.1) and (9.2) to a finite value. .

Then we can apply the standard Matrix method to the coupled integro-differential equations by dividing the energy range of Γ valley into n intervals and the L valley into n intervals also. Thus we have a vector of distribution function of f with $n+1$ elements for Γ valley and $n+1$ elements for L valley. The integral in the coupled equations (9.2) and (9.3) then equals the summation of

subregional integrals.

$$\begin{aligned} \frac{\partial f_{\Gamma}(\epsilon_i)}{\partial t} &= \sum_{j=1}^{n+1} \int_{\epsilon_j}^{\epsilon_{j+1}} d\epsilon_{k'} [S_{\Gamma, \Gamma}(\epsilon_i, \epsilon_{k'}) (f_{\Gamma}(\epsilon_i) - \frac{f_{\Gamma, eq}(\epsilon_i)}{f_{\Gamma, eq}(\epsilon_{k'})} f_{\Gamma}(\epsilon_{k'})) \\ &+ S_{L, \Gamma}(\epsilon_i, \epsilon_{k'}) f_{\Gamma}(\epsilon_i)] - \sum_{j=n+1}^{2n+2} \int_{\epsilon_j}^{\epsilon_{j+1}} d\epsilon_{k'} S_{L, \Gamma}(\epsilon_i, \epsilon_{k'}) \frac{f_{\Gamma, eq}(\epsilon_i)}{f_{L, eq}(\epsilon_{k'})} f_L(\epsilon_{k'}) \end{aligned} \quad (9.14)$$

for $i = 1, n + 1$, and

$$\begin{aligned} \frac{\partial f_L(\epsilon_i)}{\partial t} &= - \sum_{j=1}^{n+1} \int_{\epsilon_j}^{\epsilon_{j+1}} d\epsilon_{k'} S_{\Gamma, L}(\epsilon_i, \epsilon_{k'}) \frac{f_{L, eq}(\epsilon_i)}{f_{\Gamma, eq}(\epsilon_{k'})} f_{\Gamma}(\epsilon_{k'}) \\ &+ \sum_{j=n+2}^{2n+2} \int_{\epsilon_j}^{\epsilon_{j+1}} d\epsilon_{k'} [S_{L, L}(\epsilon_i, \epsilon_{k'}) (f_L(\epsilon_i) - \frac{f_{L, eq}(\epsilon_i)}{f_{L, eq}(\epsilon_{k'})} f_L(\epsilon_{k'})) \\ &+ S_{\Gamma, L}(\epsilon_i, \epsilon_{k'}) f_L(\epsilon_i)] \end{aligned} \quad (9.15)$$

for $i = n + 2, 2n + 2$.

The right hand side of (9.14) and (9.15) can be expressed as $\mathbf{S}\hat{f}$. \mathbf{S} is a matrix with elements corresponding to the subregional integrals in (9.14) and (9.15). These subregional integrals are easy to calculate because of the δ functions in (9.4-7), the coupled L and Γ valley rate equations can be expressed by

$$\frac{\partial \hat{f}}{\partial t} = \mathbf{S}\hat{f} \quad (9.16)$$

This linear system can be solved¹⁰⁸ by obtaining the eigenvalue λ_j and corresponding eigenvector \hat{V}_{ij} of the matrix \mathbf{S} , then the energy distribution

$$f(\epsilon_i) = \sum_j a_j V_{ij} e^{\lambda_j t} \quad (i, j = 1 \cdots 2n + 2) \quad (9.17)$$

a_j is the coefficient to be determined by the initial condition. V_{ij} is the i th element in eigenvector \hat{V}_j .

Substitute the initial distribution to (9.16), we need to solve a set of linear algebraic equations

$$\sum_j V_{ij} a_j = f_0(\epsilon_i) \quad (9.18)$$

i.e.

$$\mathbf{V} \hat{\mathbf{a}} = \hat{\mathbf{f}}_0 \quad (9.19)$$

to obtain the coefficients in (9.16).

CHAPTER 10 RELAXATION PROCESSES

10.1 Numerical Results

The time evolution of the distribution function during the first $60fs$ after excitation in bulk GaAs in the Γ valley is shown in Fig.11(a). The main effect on this time scale is the reduction in the number of electrons that are in the heavy and light hole peaks. This reduction comes primarily from the transfer of electrons into the L valleys. There is some transfer into the X valleys, but this is negligible compared to scattering into the L valleys since the X valley is higher in energy. The distributions of electrons for the same time scales from the Monte Carlo simulation⁴⁰ are also presented in Fig.11(a). One can see that the distributions obtained by the matrix method agree extremely well with those obtained from the more computationally intensive Monte Carlo approach. Fig.11(b) shows the distribution functions in L valley of the same time scale. The two peaks are corresponding to the reduction of initial excitations in Γ valley due to the intervalley scattering.

Fig.12(a) shows the energy distribution in Γ valley for $100fs$ to $400fs$ after initial excitation. On this time scale, we see a lowering of the total energy of the distribution. This occurs mainly through polar optical phonon and $L - \Gamma$ scattering. As can be seen from the Fig.12(a), there is a decrease in the number of electrons in the OCR on the time scale as electrons emit polar optical phonons and are scattered out of the OCR. Fig.12(b) shows the

distribution functions in L valley in the same time scale. We can also see the lowering of the total energy of the electrons compared with Fig.11(b).

Fig.13(a) shows the energy distributions in Γ valley for 1000 – 3000 fs after initial excitation. The energy distributions in L valley for the same time scale are shown in Fig.13(b), the electrons relax to a thermal-like distribution.

The distribution function of hot electrons $f(\epsilon_c)$ can be obtained from the hot electron photoluminescence spectrum.¹⁰² The particular shape of the spectrum is determined by the distribution function of the photoexcited electrons, acceptor holes and also by the transition probability. The energy distribution of the free carriers can be reconstructed from the spectrum of the band-impurity radiative recombination, provided that the probability for the corresponding transition is known. This probability is proportional to the square of the modulus of the carrier wave function at the center in the momentum representation. The band to acceptor transition probability is approximated by¹⁰³

$$|a(k)|^2 \propto 1/(1+x)^4 \quad (10.1)$$

where $x = m_c \epsilon_c(k)/m_A \epsilon_A$, m_c and $\epsilon_c(k)$ are the mass and the energy of electrons in the Γ minimum, ϵ_A is the acceptor ionization energy and m_A is the hole mass. A simple relation is valid between luminescence energy $\hbar\omega$ and ϵ_c : $\epsilon_c = \hbar\omega - (\Delta - \epsilon_A)$.

The density distribution of electrons in Γ valley averaged over 7000 fs after initial excitation obtained by matrix method is shown in Fig.14. For comparison, the function $n(\epsilon_c) = f(\epsilon_c)g(\epsilon_c)$ evaluated¹⁰⁹ from the hot electron photoluminescence spectrum is shown in the same figure, here $g(\epsilon_c)$ is the density of states. One can see that oscillations occur in the distribution functions and agree with those obtained from luminescence spectrum. The separation in

energy between the peaks of the electron distribution in the conduction band clearly shows the role of the polar optic phonon scattering in the relaxation process. A weak shoulder-like feature near $\epsilon = 300meV$ in the distribution function is very similar to that occurs in the experimental spectrum. It seems that the shoulder-like feature is related to the $\Gamma - L$ transition accompanied by the emission of optical phonons and is not necessary due to the emission of TA phonons as originally suggested.¹⁰²

The separation in energy between the peaks of the electron distribution is decided by the energy of polar optical phonons, hence the oscillational feature is not very sensitive to the temperature. The hot electron photoluminescence spectrum obtained in the experiment for liquid nitrogen temperature is of the same nature as that at liquid helium temperature.⁹¹ The calculation result of density distribution for temperature at $T=20K$ is shown in Fig.15.

10.2 Nonparabolicity

For values of k far from the minima of the conduction band and from the maxima of the valence band, the energy deviates from the simple quadratic expression, and nonparabolicity occurs.^{3,92}

For the conduction band, a simple analytical way of introducing nonparabolicity is to consider an energy wave vector relation of this type.⁹²

$$\epsilon(1 + \alpha\epsilon) = \frac{\hbar^2 k^2}{2m} \quad (10.2)$$

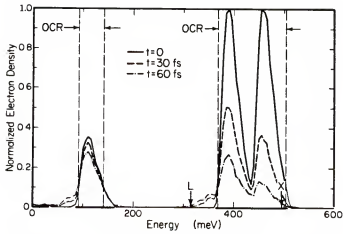
α is a nonparabolic parameter, for bulk GaAs, $\alpha = 0.64/\epsilon V$ (in table 2.2 Ref.92), then

$$d\epsilon(1 + 2\alpha\epsilon) = \frac{\hbar^2}{m} k dk \quad (10.3)$$

The effect of nonparabolicity on density of states can be calculated by

$$\int_0^{\infty} k^2 dk = \int_0^{\infty} d\epsilon \frac{2^{\frac{1}{2}} m^{*\frac{3}{2}}}{\hbar^3} \epsilon^{\frac{1}{2}} (1 + \alpha\epsilon)^{\frac{1}{2}} (1 + 2\alpha\epsilon) \quad (10.4)$$

The nonparabolicity of band structure does not change the main features of the distribution function, see Fig.16. But it should be considered for detail comparison with the shape of photoluminescence spectrum.



The energy distribution of photoexcited electrons in bulk GaAs in the Γ valley from Ref. 96 during the first 60 fs after excitation in 20 fs intervals.

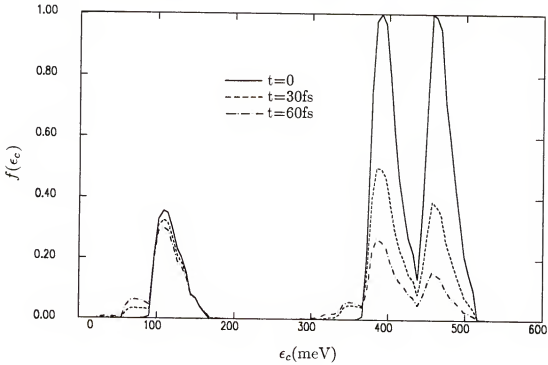


FIG. 11(a). The energy distribution of photoexcited electrons in bulk GaAs in the Γ valley during the first 60 fs after excitation in 20 fs intervals. For comparison, the upside graph shows the results from the Monte Carlo approach.

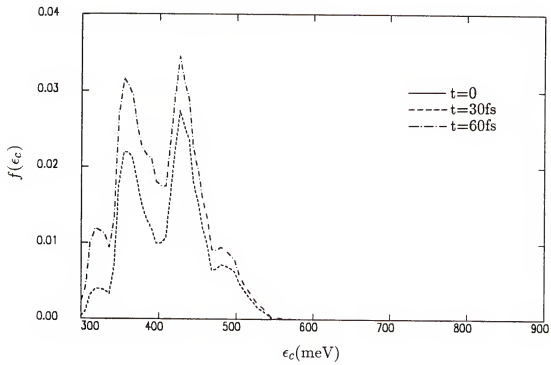
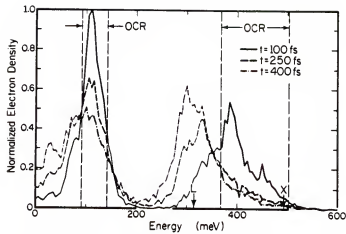


FIG. 11(b). The energy distribution of photoexcited electrons in bulk GaAs in the L valley during the first 60 fs after excitation in 20 fs intervals.



The energy distribution of photoexcited electrons in bulk GaAs in the Γ valley from Ref. 96 for 100 – 400 fs after excitation.

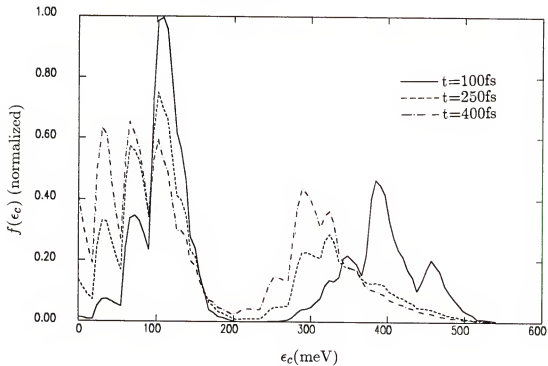


FIG. 12(a). The energy distribution of photoexcited electrons in bulk GaAs in the Γ valley for 100 – 400 fs after excitation. For comparison, the upside graph shows the results from the Monte Carlo approach.

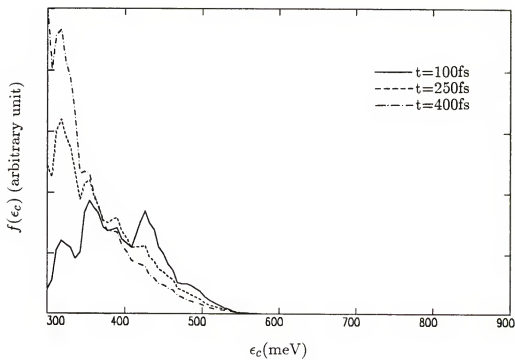


FIG. 12(b). The energy distribution of photoexcited electrons in bulk GaAs in the L valley for 100 – 400 fs after excitation.

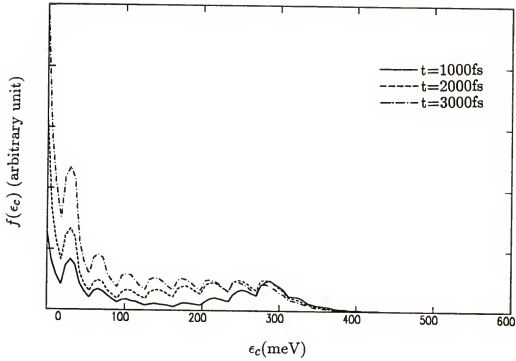


FIG. 13(a). The energy distribution of photoexcited electrons in bulk GaAs in the Γ valley for 1000 – 3000 fs after excitation.

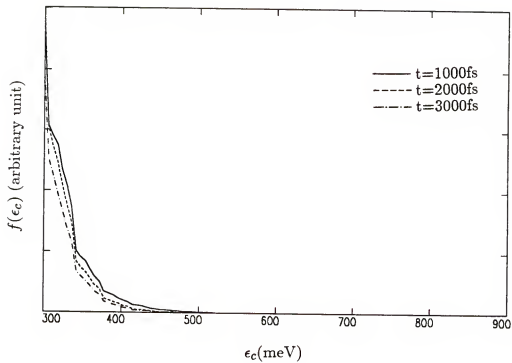
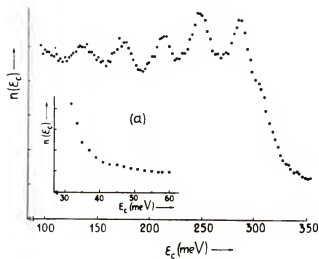


FIG. 13(b). The energy distribution of photoexcited electrons in bulk GaAs in the L valley for 1000 – 3000 f_s after excitation.



The distribution function of photoexcited electrons from Ref. 109.

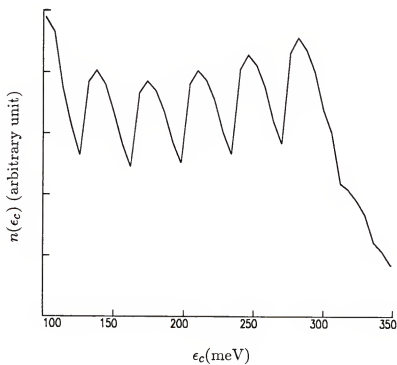


FIG. 14. The density distribution of photoexcited electrons in bulk GaAs in the Γ valley averaged over $7000fs$ after excitation.

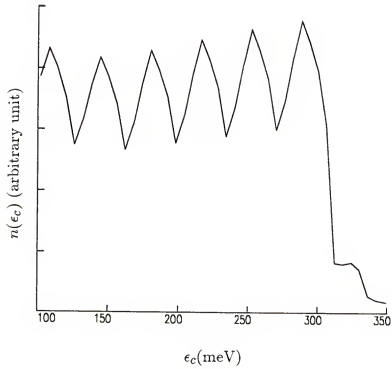


FIG. 15. The density distribution of photoexcited electrons in bulk GaAs in the Γ valley averaged over $7000fs$ after excitation at effective temperature $T = 20K$.

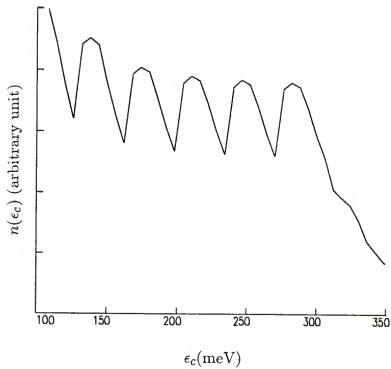


FIG. 16. The density distribution of photoexcited electrons in bulk GaAs in the Γ valley averaged over $7000fs$ after excitation at effective temperature $T = 300K$, the nonparabolicity effects are taken into account.

CHAPTER 11 SUMMARY AND DISCUSSION

In summary, in the first part of the dissertation we have solved the kinetic equations of the quasiparticles for superfluid $^3\text{He-B}$ and the phonons of ^4He and obtained the temperature and normal velocity distributions by using conservation laws and introducing the chemical potential μ_n of the quasiparticles in ^3He . We have also investigated the effective hydrodynamic boundary condition for a superfluid-normal fluid counterflow problem, assuming a diffuse scattering mechanism at the boundary and neglecting the deformation of the order parameter near the boundary. We obtain for the first time the macroscopic boundary condition and the thermal boundary resistance in the hydrodynamic regime, as well as the thermal counterflow in the Knudsen regime. In the hydrodynamic regime the Kapitza temperature jump at the wall is in general small compared to the temperature variations within the fluid.

In essence, in ^3He almost all the heat load leaves the surface in the form of diffusion current proportional to a temperature gradient, whereas in ^4He , for T not too close to T_c , the heat is carried by the normal fluid flow. This conclusion is important in explaining two extreme situations. Firstly, in the study of sound propagation in $^4\text{He II}$, one may follow Khalatnikov²⁴ to give the whole load of thermal transport to $v_n = f/s$. Secondly, the other extreme, with $v_s = v_n = 0$ in the rest frame at the interface where T' carries the whole load, Brand and Cross¹⁰⁴ were able to account for the large damping that is observed in U-tube experiments¹⁰⁵ of superfluid ^3He .

More realistic boundary conditions are needed for the quantitative comparison with the experimental results.

(i) Boundary with both diffuse and specular scatterings. For a microscopically rough surface one may expect elastic scattering with a broad angular distribution to be dominant. For the transverse flow, by assuming purely diffuse scattering one may account for only part of the discrepancy¹⁰⁶ of the viscosity in the pseudoisotropic B phase of superfluid ^3He between experimental results¹⁰ and theoretical prediction.¹⁰⁷ For the case of superfluid-normal fluid counter flow normal to the surface, the effects of specular scattering need to be further investigated.

(ii) Andreev scattering. A microscopic treatment of Andreev scattering for the case of a specularly scattering surface has been given by Kieselmann and Rainer.²⁸ It has also been considered in the context of quasiparticle ballistics in the A phase¹⁰⁸ and at the A-B phase transition.¹⁰⁹ At low temperature one has to take into account the effect of the suppression of the order parameter near a solid boundary on the scattering of Bogoliubov quasiparticles. It has been shown²⁶ that this scattering process increases the transverse flow of excitations between parallel plates and determines the damping in a torsional-oscillator experiment.¹⁸ The consideration of Andreev scattering in our problem is given in Appendix C.

However, we speculate that the effective boundary condition will be essentially unchanged for the following reasons. In ^3He the amount of heat carried by the wall via normal flow is being controlled by v_n . The slip length however, is expected to be of the order of mean-free path, and therefore so long as $L \gg \ell(T)$, it is always a good approximation to have $v_n \sim 0$ at the boundary. The normal fluid heat flow near the boundary will be important only when this

slip length and hence ℓ is comparable to L , i.e. when we approach the Knudsen regime, where the hydrodynamic approach itself fails. We expect Andreev reflections will increase this slip length, but we do not expect that this length will become macroscopically large. This speculation is in agreement with the analysis of the U-tube experiment,¹⁰⁴ where one can account for the damping observed by assigning the entire heat load at the surface to the gradient in temperature and putting $v_n = 0$ at the boundary.

In ^4He , when T is not too close to T_c , effectively we are always “outside the s-q mode”, and therefore the heatflow is essentially all carried by the normal flow. This is expected to be a general feature, except when $T \rightarrow T_c$ where $\lambda(T)$ diverges.

In the second part of the dissertation we have calculated the transient distribution functions of laser-excited electrons in the Γ and L valleys by solving a set of coupled Boltzmann integro-differential equations. The electron-polar optical phonon and $\Gamma - L$ intervalley deformation potential scattering mechanisms are taken into account. The fast relaxation process is dominated by $\Gamma - L$ scattering. On the intermediate time scale, the Γ valley electrons lose energy mainly by optical phonon emissions. The distribution functions obtained from matrix method agree extremely well with those obtained from the more computationally intensive Monte Carlo approach. On a longer time scale, oscillations occur in the distribution functions and agree with those obtained from hot luminescence spectrum. The separation in energy between the peaks of the electron distribution in the conduction band clearly shows the role of polar optical phonon scattering in the relaxation processes. Our results also show that a shoulder-like feature in the luminescence spectrum near 300meV

is related to the $\Gamma - L$ transition accompanied by the emission of polar optical phonons and is not due to the emission of TA phonons as originally suggested.

A number of unsolved questions in the simulation of the femtosecond relaxation processes have been discussed in Ref.40. Here we mention those dealing with approximations made in performing theoretical modeling.

In the calculations we have neglected the role of holes in determining the transmission spectra. Away from the band edge the nonlinear absorption is proportional to

$$\alpha = \alpha_0(1 - f_e(t) - f_h(t)) \quad (11.1)$$

Thus measuring the transmission of the probe pulse provides information on both the electron distribution and the hole distribution. Neglecting the effect of the hole distribution function on the femtosecond relaxation spectra is a major assumption that is not necessarily valid, but is based on the following reasons. Because of larger effective masses, the hole OCR is close to the valence bands, and the holes are closer in energy to thermal equilibrium than the photoexcited electrons. Also the hole-hole and hole-phonon scattering rates are significantly faster than the electron-electron and electron-phonon scattering rates³⁸. From estimates of electron-electron scattering, the hole scattering time should be on the order of tens of femtoseconds. Since the holes scatter more often and are close to equilibrium, the estimated effect of the holes on the relaxation spectra occurs on a very short time scale, typically quicker than the duration of the pump pulse. This makes it difficult to observe the effect of the hole thermalization in pump-prob experiments where pump and probe are at the same energy. However, if the probe is at a different energy as in the recent femtosecond pump-continuum probe experiments,¹¹⁻¹⁶ then the effects of the holes might be observable. Once the holes thermalize, it is the electrons

which are the dominant contribution to the femtosecond spectra. Further work is needed to determine the extent to which holes affect the femtosecond transmission spectra.

Another effect neglected in our calculations is band gap renormalization (narrowing) as the electrons are excited into the conduction band by the pump pulse. Typically in bulk GaAs for doped semiconductors is estimated¹¹² to be about 12meV for density of 10^{17}cm^{-3} , and has been observed as a function of time as the electrons are injected into the conduction band.¹¹³ How the band gap renormalization changes for electrons injected with energies high above the band bottom is not well known. If it is the same or lower than the band bottom, one may expect a $10 - 15\text{meV}$ shift in the band gap during a high-intensity pump pulse changing the OCR measured by the probe pulse. In the experiment,³³ the OCR is at least 35meV wide in bulk GaAs. Therefore, a 15meV shift in the band gap should not significantly alter the calculation results. However, more calculations are needed to verify this.

Since the photoexcited electrons are highly nonequilibrium and can not be properly characterized by an effective temperature, the uniform temperature which we defined in the phonon distribution function introduced in this calculation is only a kind of approximation. The energy separation between the peaks of the oscillations in the distribution of photoexcited electrons is decided by the polar optical phonon frequency. The temperature of the phonons affects the shape of the distribution as shown in Fig.15. Hence it may be considered as a possible method to determine the effective temperature of the approximate equilibrium phonons by comparison of the calculation results with the luminescence spectrum.

The initial distribution of laser excited electrons in this calculation is under such assumption that the laser pulse is instantaneous. A more realistic model of laser beam is a continuous wave as $\cos^2\omega t$ type. This effect should be taken into account for further calculation.

Recently the dependence of the intensity of heavy hole peak of hot luminescence on the laser photon energy has been measured.¹¹⁴ This relation can also be obtained by extending our present calculation to different laser energies. In doing so we need to calculate the initial distribution of photoexcited electrons by using the $\mathbf{k} \cdot \mathbf{p}$ matrix¹¹⁵, the double- δ -function integral¹¹⁶ and the appropriate optical transition matrix elements⁹¹ as discussed in Ref.117.

Hot electron luminescence spectrum has been used to obtain the band structure information and the deviation from the $\mathbf{k} \cdot \mathbf{p}$ calculations.¹¹⁷⁻¹¹⁹ The determination of the intervalley scattering rate by the hot electron photoluminescence spectrum¹¹⁴ needs further investigations.

APPENDIX A
LANDAU-BOLTZMANN EQUATION

For slowly varying phenomena in space and time, the wavelength of the disturbance is much longer than the Fermi wavelength $\lambda_F = 2\pi/k_F$ and the frequency is much less than the Fermi frequency, the quasiparticles may be considered as classical objects.¹²⁰ The change in time of the distribution function $n_{\vec{k}}$ is then given by

$$i\hbar \frac{\partial}{\partial t} \langle k | n | k' \rangle = \langle k | [\epsilon, n] | k' \rangle \quad (\text{A.1})$$

where $\langle k | n(t) | k' \rangle = \langle a_{\vec{k}}^\dagger a_{\vec{k}'} \rangle$ is the distribution function matrix in momentum space in a nonequilibrium state. It is convenient to introduce the mixed representation, where the particle-hole amplitude $\langle a_{\vec{k}}^\dagger a_{\vec{k}'} \rangle$ is described in terms of relative and total coordinates

$$n_{\vec{k}}(\vec{r}, t) = \sum_{\vec{q}} e^{i\vec{q}\cdot\vec{r}} \langle a_{\vec{k}+\frac{\vec{q}}{2}}^\dagger a_{\vec{k}-\frac{\vec{q}}{2}} \rangle \quad (\text{A.2})$$

The function $n_{\vec{k}}(\vec{r}, t)$ describes the local momentum distribution in space and time. The energy operator is given by its matrix $\langle \vec{k} | \epsilon | \vec{k}' \rangle$. Then consider a quadratic term, $\langle k | \hat{n}\hat{\epsilon} | k' \rangle$, take $\vec{k} \rightarrow \vec{k} + \frac{\vec{q}}{2}$ and $\vec{k}' \rightarrow \vec{k} - \frac{\vec{q}}{2}$,

$$\langle k | \hat{n}\hat{\epsilon} | k' \rangle = \sum_{\vec{Q}} \langle \vec{k} + \frac{\vec{q}}{2} | \hat{n} | \vec{k} - \frac{\vec{q}}{2} + \vec{Q} \rangle \langle \vec{Q} + \vec{k} - \frac{\vec{q}}{2} | \hat{\epsilon} | \vec{k} - \frac{\vec{q}}{2} \rangle \quad (\text{A.3})$$

here we introduce $\epsilon_{\vec{k}}(\vec{r}, t)$ as the local quasiparticle energy.

$$\begin{aligned} & \langle k | \hat{n}\hat{\epsilon} | k' \rangle \\ &= \sum_{\vec{Q}} \int d^3r_1 n_{\vec{k}+\frac{\vec{q}}{2}}(\vec{r}_1, t) e^{i(\vec{Q}-\vec{q})\cdot\vec{r}_1} \int d^3r_2 \epsilon_{\vec{k}+\frac{\vec{Q}-\vec{q}}{2}}(\vec{r}_2, t) e^{-i\vec{Q}\cdot\vec{r}_2} \end{aligned} \quad (\text{A.4})$$

Expand in small \vec{q}, \vec{Q} ,

$$n_{\vec{k}+\frac{\vec{q}}{2}} = n_{\vec{k}} + \frac{1}{2}\vec{Q} \cdot \vec{\nabla}_k n_{\vec{k}} \quad (\text{A.5})$$

$$\epsilon_{\vec{k}+\frac{\vec{q}-\vec{f}}{2}} = \epsilon_{\vec{k}} + \frac{1}{2}(\vec{Q} - \vec{q}) \cdot \vec{\nabla}_k \epsilon_{\vec{k}} \quad (\text{A.6})$$

then

$$\begin{aligned} \langle k | \hat{n} \hat{\epsilon} | k' \rangle &= \sum_{\vec{Q}} \int d^3 r_1 d^3 r_2 [n_{\vec{k}} + \frac{i}{2}\vec{\nabla}_k n_{\vec{k}} \vec{\nabla}_2] e^{-i\vec{Q} \cdot \vec{r}_2} \\ &\cdot [\epsilon_{\vec{k}} - \frac{i}{2}\vec{\nabla}_k \epsilon_{\vec{k}} \vec{\nabla}_1] e^{i(\vec{Q}-\vec{q}) \cdot \vec{r}_1} \end{aligned} \quad (\text{A.7})$$

and

$$\begin{aligned} \sum_{\vec{q}} e^{i\vec{q} \cdot \vec{r}} \langle k | \hat{n} \hat{\epsilon} | k' \rangle &= \int d^3 r_1 d^3 r_2 [n_{\vec{k}}(\vec{r}_1) \epsilon_{\vec{k}}(\vec{r}_2) - \frac{i}{2}\vec{\nabla}_k n_{\vec{k}} \vec{\nabla}_2 \epsilon_{\vec{k}} \\ &+ \frac{i}{2}\vec{\nabla}_k \epsilon_{\vec{k}} \vec{\nabla}_1 n_{\vec{k}} + \text{highorder}] \delta^3(\vec{r} - \vec{r}_1) \delta^3(\vec{r}_1 - \vec{r}_2) \end{aligned} \quad (\text{A.8})$$

For $\langle k | \hat{n} \hat{\epsilon} | k' \rangle$, we can do similar calculation and obtain the Landau-Boltzmann equation

$$\frac{\partial}{\partial t} n_{\vec{k}}(\vec{r}, t) + \vec{\nabla}_k \epsilon_{\vec{k}}(\vec{r}, t) \vec{\nabla}_r n_{\vec{k}}(\vec{r}, t) - \vec{\nabla}_k n_{\vec{k}}(\vec{r}, t) \vec{\nabla}_r \epsilon_{\vec{k}}(\vec{r}, t) = I_{\vec{k}}\{n_{\vec{k}}\} \quad (\text{A.9})$$

Effects of dissipation are accounted for by the collision integral $I_{\vec{k}}$

$$\begin{aligned} I_{\vec{k}\sigma}\{n_{\vec{n}}\} &= 2\pi \sum_{\vec{k}_2 \vec{k}_3 \vec{k}_4 \sigma_2} |\langle \vec{k} \vec{k}_2 | T | \vec{k}_3 \vec{k}_4 \rangle|^2 \{n_{\vec{k}} n_{\vec{k}_2} (1 - n_{\vec{k}_3}) (1 - n_{\vec{k}_4}) \\ &- (1 - n_{\vec{k}}) (1 - n_{\vec{k}_2}) n_{\vec{k}_3} n_{\vec{k}_4}\} \delta(\epsilon_{\vec{k}} + \epsilon_{\vec{k}_2} - \epsilon_{\vec{k}_3} - \epsilon_{\vec{k}_4}) \\ &\cdot \delta(\vec{k} + \vec{k}_2 - \vec{k}_3 - \vec{k}_4) \delta(\sigma + \sigma_2 - \sigma_3 - \sigma_4) \end{aligned} \quad (\text{A.10})$$

APPENDIX B
ONSAGER RELATION

The energy flux normal to the interface, to quadratic order, and with vanishing shear flow, is given as²²

$$Q_L = T_L f_L + (\alpha v'_n + \beta g') j_s / \rho \quad (\text{B.1})$$

for the superfluid on the left (L), $x < 0$, and

$$Q_R = T_R f_R \quad (\text{B.2})$$

for the solid on the right (R), $x > 0$. Here, $j_s = \rho_s(v_s - v_n)$, α , β are combinations of shear viscosity η and second viscosities $\zeta_{1,2,3}$: $\alpha = \frac{4}{3}\eta - 2\zeta_1\rho + \zeta_2 + \zeta_3\rho^2$, $\beta = \zeta_1 - \zeta_3\rho$. An additional summand in Q_R , proportional to the longitudinal component of the stress field has been set equal to zero, because since it is a measure of the energy required for displacing a particle from the bulk solid to the surface,¹²¹ it should vanish at the interface. Besides, keeping it only leads to a boundary condition for the solid. Another summand $\sim g$ was eliminated by going to the rest frame of the interface (only when one deals with melting or evaporation^{122–124} is the mass current across the interface nonzero). The mass and entropy flow, g_0 and f_0 in the rest frame are related to the respective quantities of the lab frame by $g_0 = g - \rho u = 0, f_0 = f - su = -\sigma j_s - \kappa T'/T$, where u is the interface velocity. Now, the energy flux in the rest frame is continuous across the interface; hence

$$R_s \equiv -T\Delta f_0 = f_0\Delta T + (\alpha v'_n + \beta g') j_s / \rho \quad (\text{B.3})$$

where $\Delta A \equiv A_L - A_R$ and $A \equiv (A_L + A_R)/2$ for T and f_0 , and R_s/T denotes the surface entropy production. Therefore we can set

$$f_0 = a\Delta T + c(\alpha v'_n + \beta g^l)/\rho \quad (\text{B.4})$$

$$j_s = c\Delta T + b(\alpha v'_n + \beta g^l)/\rho \quad (\text{B.5})$$

with the surface Onsager coefficients $a, b > 0$, and $c^2 \leq ab$. Eq.(B.4), (B.5) and $g = \rho u$ are the most general boundary conditions compatible with conservation laws and irreversible thermodynamics.

APPENDIX C
BOUNDARY CONDITION FOR $\delta f_p^{(+)}$

For general consideration of the microscopic boundary condition, we introduce distribution function $f_p^{(+)}(x)$ for quasiparticles moving away from the wall (velocity $v_x > 0$) and $f_p^{(-)}(x)$ for quasiparticles moving towards the wall ($v_x < 0$). At the wall we assume the distribution functions $\delta f_p^{(+)}$ and $\delta f_p^{(-)}$ to be related by^{9,22}

$$f_p^{(+)}(0) = \frac{1}{|v_{p_x}|} \sum_{\substack{p' \\ v_{p'_x} < 0}} (p | R | p') |v_{p'_x}| f_{p'}^{(-)}(0) \quad (\text{C.1})$$

here the quantity $(p | R | p')$ is the transition probability for scattering of quasiparticles from momentum state $|p'\rangle$ to state $|p\rangle$ and is independent of the deviation from global equilibrium.

We treat only the case when the scattering conserves particle number. Under stationary condition the incoming and outgoing total particle current density must be equal, consequently we have the normalization condition

$$\sum_{\substack{p \\ v_{p_x} > 0}} (p | R | p') = 1 \quad (\text{C.2})$$

so that

$$\sum_{\substack{p \\ v_{p_x} > 0}} |v_{p_x}| f_p^{(+)}(0) = \sum_{\substack{p' \\ v_{p'_x} < 0}} |v_{p'_x}| f_{p'}^{(-)}(0) \quad (\text{C.3})$$

generally $(p | R | p')$ can consist different scattering mechanisms, diffuse, specular, Andreev, et al.. The scattering function must be nonnegative. Furthermore, the global equilibrium distribution f_p^0 must obey (C1). A sufficient

condition for this is

$$(p | R | p') | v_{p'_x} | f_p^0 = (-p' | R | -p) | v_{p_x} | f_p^0 \quad (\text{C.4})$$

for $v_{p_x} > 0$, $v_{p_x} < 0$. This is the reciprocity relation for boundary scattering.¹

In the case of elastic scattering the transition probability include a delta function ensuring conservation of local energy.

$$(p | R | p') = (p | \tilde{R} | p') \delta[E_p(\vec{r}, t) - E_{p'}(\vec{r}, t)] \quad (\text{C.5})$$

where $E_p(r, t)$ may contain the effect of the local chemical potential, velocity field or magnetic field. For the special case of completely diffuse scattering at the boundary, the simplest possible model for the transition probability is given by

$$(p | R | p') = | v_{p_x} | R_0 \delta(E_p - E_{p'}) \quad (\text{C.6})$$

where $R_0 = (v_F N_F / 4)^{-1}$ from the normalization condition (c2). However it is more convenient to directly write down $f_p^{(+)}$, since by definition, $f_p^{(+)}(0)$ is in equilibrium with the wall

$$\begin{aligned} f_p^{(+)}(0) &= f^0((E_p + \delta E_p)/(T + \delta T)) \\ &= f^0(E_p) + f_p'(\delta E_p - \frac{E}{T} \delta T_L) \end{aligned} \quad (\text{C.7})$$

then

$$\delta f_p(0) = f_p'(\delta E_p - \frac{E}{T} \delta T_L) \quad (\text{C.8})$$

From

$$\delta f_p'(0) = \delta f_p(0) - f_p'(\delta E_p - p_x v_n(0) - E_p \frac{\delta T(0)}{T}) \quad (\text{C.9})$$

we can obtain

$$\delta f_p'(0) = f_p'(p_x v_n(0) + E_p \frac{\delta T(0) - \delta T_L}{T}) \quad (\text{C.10})$$

and

$$\begin{aligned}\delta f_p^{(+)}(0) &= \delta f_p'(0) + f_p' \frac{\xi_p}{E_p} \delta \mu_n \\ &= f_p'(p_x v_n(0) + \frac{\xi_p}{E_p} \delta \mu_n + E_p \frac{\delta T(0) - \delta T_L}{T})\end{aligned}\quad (\text{C.11})$$

generally we can write down the distribution function as

$$\begin{aligned}f_p^{(+)}(0) &= \alpha(f(E_p) + f_p'(E_p - \frac{E_p}{T} \delta T_L)) \\ &+ \frac{1}{|v_{p_x}|} \sum_{\substack{p' \\ v_{p'_x} < 0}} (p | R | p') | v_{p'_x} | f_{p'}^{(-)}(0)\end{aligned}\quad (\text{C.12})$$

$0 < \alpha$ is the fraction of diffuse scatterings, $(p | R | p')$ is the “remainder” of the reflections. The renormalization condition with the conservation of Bogoliubov quasiparticle number becomes

$$\begin{aligned}\alpha \sum_{\substack{p \\ v_{p_x} > 0}} |v_{p_x}| (f(E_p) + f_p'(\delta E_p + E_p \frac{\delta T_L}{T})) \\ + \sum_{\substack{p' \\ v_{p'_x} < 0}} [\sum_{\substack{p \\ v_{p_x} > 0}} (p | R | p') - 1] |v_{p'_x}| f_{p'}^{(-)} = 0\end{aligned}\quad (\text{C.13})$$

At low temperature one has to take into account the effect of the suppression of the order parameter near a solid boundary on the scattering of Bogoliubov quasiparticles. As first shown by Andreev⁸⁰ for *s*-wave superconductors, quasiparticles close to the gap edge are reflected from a solid wall by action of the spatial variation of the gap parameter. It is remarkable that this reflection process take place via a transition from one particle-hole branch, where $\xi_p > 0$, to the other one with $\xi_p < 0$, such that the group velocity is reversed $\vec{v}_p \rightarrow -\vec{v}_{p'}$, but the momentum \vec{p} is hardly changed. We may describe these processes by a model form for the transition probability

$$(\vec{p} | R | -\vec{p}')_A = N_F^{-1} R_A(E_p) \delta(\xi_p + \xi_{p'}) \delta(\vec{p} - \vec{p}') \quad (\text{C.14})$$

where N_F is the density of states at the Fermi level.

The reflection amplitude $R_A(E_p)$ may be calculated from the Bogoliubov-de Gennes equations once the gap profile $\Delta(x)$ is known⁸². More fundamentally, $R_A(E)$ follows from a self-consistent treatment of the boundary value problem.^{125,126}

REFERENCES

1. C. Cercignani, *Theory and Application of the Boltzmann Equation* (Scottish Academic, Edinburgh, 1975).
2. E.M. Lifshitz and L.P. Pitaevskii, *Physical Kinetics* (Pergamon Ltd, Oxford, 1981).
3. C. Jacoboni and L. Reggiani, *Rev. Mod. Phys.* 55, 645 (1983).
4. N.S. Wingreen, C.J. Stanton, and J.W. Wilkins, *Phys. Rev. Lett.* 57, 1084 (1986).
5. G.S. Canright and G.D. Maham, *Phys. Rev.* B36, 1025 (1987).
6. C.S. Kim, J.W. Dufty, A. Santos, and J.J. Breg, *Phys. Rev.* A39, 328 (1989).
7. H. Smith, *Physica (Amsterdam)* 126B+C, 267 (1984).
8. J.P. Eisenstein, G.W. Swift, and R.E. Packard, *Phys. Rev. Lett.* 45, 1199 (1980).
9. J.M. Parpia, D.J. Sandiford, J.E. Berthold, and J.D. Reppy, *Phys. Rev. Lett.* 40, 565 (1978).
10. C.N. Archie, T.A. Alvesalo, J.D. Reppy, and R.C. Richardson, *J. Low Temp. Phys.* 42, 295 (1980).
11. D.C. Carless, H.E. Hall, and J.R. Hook, *J. Low Temp. Phys.* 50, 605 (1983).
12. A.W. Yanof and J.D. Reppy, *Phys. Rev. Lett.* 33, 631 (1974).
13. T. Chainer, Y. Morii, and H. Kojima, *Phys. Rev.* B21, 3941 (1980).
14. G. Eska, K. Neumaier, W. Schoepe, K. Uhlig, W. Wiedemann, and P. Wölffe, *Phys. Rev. Lett.* 44, 1337 (1980).
15. T. Kodama and H. Kojima, *Phys. Lett.* A87, 103 (1981).
16. C. Cercignani, in *Rarefield Gas Dynamics*, edited by J.A. Laurmann (Academic, New York, 1963), Vol.2.
17. J.E. Jaffe, *J. Low Temp. Phys.* 37, 567 (1979).

18. H. Højgaard Jensen, H. Smith, P. Wölffe, K. Nagai, and T. Maack Bisgaard, *J. Low Temp. Phys.* 41, 473 (1980).
19. D. Einzel, H. Højgaard Jensen, H. Smith, and P. Wölffe, *J. Low Temp. Phys.* 53, 695 (1983).
20. H. Højgaard Jensen, H. Smith and P. Wölffe, *J. Low Temp. Phys.* 51, 81 (1983).
21. F. Topsøe and H. Højgaard Jensen, *J. Low Temp. Phys.* 55, 469 (1984).
22. M. Grabinski and M. Liu, *Phys. Rev. Lett.* 58, 800 (1987).
23. M. Grabinski and M. Liu, *J. Low Temp. Phys.* 73, 78 (1988).
24. I.M. Khalatnikov, *Introduction to the Theory of Superfluidity* (Benjamin, New York, 1965).
25. J. Wilks, *The Properties of Liquid and Solid Helium* (Clarendon, Oxford, 1967).
26. D. Einzel, P. Wölffe, H. Højgaard Jensen, and H. Smith, *Phys. Rev. Lett.* 52, 1705 (1984).
27. C.J. Lambert, A.M. Guénault and G. R. Pickett, *J. Phys.* C19 L 351 (1986).
28. G. Kieselmann and D. Rainer, *Z. Phys.* B52, 267 (1983).
29. M.J. Rosker, F.W. Wise, and C.L. Tang, *Appl. Phys. Lett.* 49, 1726 (1986).
30. W.Z. Lin, J.G. Fujimoto, E.P. Ippen, and R.A. Logan, *Appl. Phys. Lett.* 50, 124 (1987).
31. R.W. Schoenlein, W.Z. Lin, S.D. Brorson, E.P. Ippen, and J.G. Fujimoto, *Appl. Phys. Lett.* 51, 1443 (1987).
32. J.L. Oudar, A. Migus, D. Hulin, G. Grillon, J. Etchepare, and A. Antonetti, *Phys. Rev. Lett.* 53, 384 (1984).
33. J.A. Kash, J.C. Tang, and J.M. Hvam, *Phys. Rev. Lett.* 54, 2151 (1985).
34. J.L. Oudar, D. Hulin, A. Migus, A. Antonetti, and F. Alexandre, *Phys. Rev. Lett.* 55, 2074 (1985).
35. M.C. Nuss, D.H. Auston, and F. Capasso, *Phys. Rev. Lett.* 58, 2355 (1987).
36. E.M. Conwell, "High field transport in semiconductors", in *Solid State Physics Advances in Research and Applications, Vol. 9*, edited by Seitz, Turnbull, and Ehrenreich (New York, 1967).
37. J. Collet, J.L. Oudar, and T. Amand, *Phys. Rev.* B34, 5443 (1986).

38. M.A. Osman and D.K. Ferry, Phys. Rev. B36, 6018 (1987).
39. D.W. Bailey, C.J. Stanton, M.A. Artaki, K. Hess, F.W. Wise, and C.L. Tang, Solid State Electron. 31, 467 (1988).
40. C.J. Stanton, D.W. Bailey, and K. Hess, IEEE J. Quantum Electron. 24, 1614 (1988).
41. D.D. Osheroff, R.C. Richardson and D. M. Lee, Phys. Rev. Lett. 28, 885 (1972).
42. A.J. Leggett, Phys. Rev. Lett. 29, 1227 (1972).
43. A.J. Leggett, Phys. Rev. Lett. 31, 352 (1973).
44. A.J. Leggett, J. Phys. C6 3187 (1973).
45. P.W. Anderson, Phys. Rev. Lett. 30, 368 (1973).
46. P.W. Anderson and W.F. Brinkman, Phys. Rev. Lett. 30, 1108 (1973).
47. P.W. Anderson and W.F. Brinkman, *The Helium Liquids*, edited by J.G.M. Armitage and I.E. Farghar (Academic, New York 1975).
48. A.J. Leggett, Rev. Mod. Phys. 47, 331 (1975).
49. L.D. Landau, Zh. Eksp. Teor. Fiz. 30, 1058 (1956) [Engl. trans., Sov. Phys. JETP 3, 920 (1956)].
50. L.D. Landau, Zh. Eksp. Teor. Fiz. 32, 59 (1957) [Engl. trans., Sov. Phys. JETP 5, 101 (1957)].
51. D. Pines and P. Nozières, *The Theory of Quantum Liquids*, (Benjamin, New York 1966).
52. A.A. Abrikosov and I.M. Khalatnikov, Rep. Prog. Phys. 22, 329 (1959).
53. A.A. Abrikosov, L.P. Gorkov, and I.E. Dzyaloshinski, *Methods of Quantum Field Theory in Statistical Physics* (Pergamon, Oxford, 1965).
54. P.W. Anderson and P. Morel, Physica 26, 671 (1960).
55. P.W. Anderson and P. Morel, Phys. Rev. 123, 1911 (1961).
56. A.J. Leggett, Phys. Rev. Lett. 14, 536 (1965).
57. A.J. Leggett, Phys. Rev. 140A, 1869 (1965).
58. V.J. Emery, Ann. Phys. (New York) 28, 1 (1964).
59. J. Bardeen, L.N. Cooper, and J. R. Schrieffer, Phys. Rev. 108, 1175 (1957).

60. N.N. Bogoliubov, V.V. Tolmachev, and D.V. Shirkov, *A New Method in the Theory of Superconductivity* (Consultants Bureau, New York, 1959).
61. R. Balian and N.R. Werthamer, *Phys. Rev.* 131, 1553 (1963).
62. W.M. Saslow, *Phys. Rev. Lett.* 31, 870 (1973).
63. G. Baym and C.J. Pethick, in *The Physics of Liquid and Solid Helium*, edited by K.H. Bennemann and J.B. Ketterson (Wiley, New York, 1977), Vol.2.
64. P. Wölfle, *J. Low Temp. Phys.* 42, 269 (1979).
65. O. Betbeder-Matibat and P. Nozières, *Ann. Phys. (New York)* 51, 392 (1969).
66. D. Einzel and P. Wölfle, *J. Low Temp. Phys.* 32, 19 (1978).
67. P. Wölfle and D. Einzel, *J. Low Temp. Phys.* 32, 39 (1978).
68. M. Pfitzner and P. Wölfle, *J. Low Temp. Phys.* 51, 535 (1983).
69. V.S. Shumeiko, *Zh. Eksp. Teor. Fiz.* 63, 621 (1972) [Engl. trans., *Sov. Phys. JETP* 36, 330 (1972)].
70. P. Wölfle, *J. Low Temp. Phys.* 26 659 (1977).
71. W.M. Saslow, *Phys. Lett.* 35A, 241 (1971).
72. J.C. Wheatley, *Rev. Mod. Phys.* 47, 415 (1975).
73. P.L. Kapitza, *Collected papers of P.L. Kapitza*, edited by D. terHaar (Pergamon, Ltd., Oxford, 1967) Vol.2, p581.
74. J.P. Harrison, *J. Low Twmp. Phys.* 37, 467 (1979).
75. I.L. Bekaravich and I.M. Khalatnikov *Zh. Eksp. Tero. Fiz.* 39, 1699 (1960) [Engl. trans., *Sov. Phys. JETP* 12, 1187 (1961)].
76. V.P. Peshkov, *Zh. Eksp. Teor. Fiz.* 46, 1510 (1964) [Engl. trans., *Sov. Phys. JETP* 19, 1023 (1964)].
77. J.C. Wheatley, *Phys. Rev.* 165, 304 (1968).
78. A.J. Leggett and M. Vuorio, *J. Low Temp. Phys.* 3, 359 (1970).
79. D.L. Mills and M.T. Béal-Monod, *Phys. Rev.* A10, 2473 (1974).
80. A.F. Andreev, *Zh. Eksp. Teor. Fiz.* 46, 1823 (1964) [Engl. trans., *Sov. Phys. JETP* 19, 1228 (1964)].
81. S. Yip, *Phys. Rev.* B32, 2915 (1985).

82. J. Kurkijarvi and D. Rainer, in *Modern Problems in Condensed Matter Sciences: Superfluid Phase of ^3He* , edited by W.P. Halperin and L.P. Pitaevskii (North-Holland, 1989).
83. D. Einzel, *J. Low Temp. Phys.* 54, 427 (1984).
84. C.A.M. Castelijns, K.F. Coates, A.M. Guénault, S.G. Mussett and G.R. Pickett, *Phys. Rev. Lett.* 55, 2021 (1985).
85. J.M. Parpia, *Phys. Rev.* B32, 7564 (1985).
86. P. Kapitza, *Nature* 141, 74 (1937).
87. L.D. Landau, *JETP* 11, 592 (1941).
88. I.M. Khalatnikov, in *The Physics of Liquid and Solid Helium*, edited by K.H. Bennemann and J.B. Ketterson (Wiley, New York, 1974).
89. A.D.B. Woods and R.A. Cowley, *Phys. Rev. Lett.*, 24, 649 (1970).
90. D.J. Ashen, P.J. Dean, D.T. Hurle, J.B. Mullin, A.M. White, and P.D. Greene, *J. Phys. Chem. Solids* 36, 1041 (1975).
91. B.P. Zakharchenya, D.N. Mirlin, V.I. Perel, and I.I. Rishin, *Usp. Fiz. Nauk* 136, 459 (1982) [Engl. trans., *Sov. Phys. Usp.* 25, 143 (1982)].
92. L. Reggiani, in *Hot-Electron Transport in Semiconductors*, edited by L. Reggiani (Springer-Verlag, Berlin Heidelberg, 1985).
93. D.E. Aspnes, *Phys. Rev.* B14, 5331 (1976).
94. K. Brennan and K. Hess, *Solid State Electron.* 27, 347 (1984).
95. M.A. Littlejohn, J.R. Hauser, and T.H. Glisson, *J. Appl. Phys.* 11, 4587 (1977).
96. N. Takenaka, M. Inone, and Y. Inuishi, *J. Phys. Soc. Japan.* 47, 861 (1979).
97. J.F. Young, P.J. Kelly, and N.L. Henry, "The effects of band structure on electron-hole coulomb scattering", in *Proc. HCIS-5 Conf.* (1988).
98. C. Jacoboni, and L. Reggiani, *Adv. Phys.* 28, 493 (1979).
99. C.J. Stanton, "Ph.D. Thesis", Cornell University (1986).
100. I.B. Levinson, *Sov. Phys. Solid State* 7, 1098 (1965).
101. W.H. Press, B.P. Flannery, S.A. Teukolsky, and W.T. Vetterling, *Numerical Recipes* (Cambridge University, New York, 1986).

102. D.N. Mirlin, I.J. Karlik, L.P. Nikitin, I.I. Reshina, and V.F. Sapega, *Solid State Commun.* 37, 757 (1981).
103. H.B. Bebb and E.W. Williams, in *Semiconductors and Semimetals*, edited by R.K. Willardson and A.C. Beer (Academic Press, New York, 1966), Vol.8.
104. H. Brand and M.C. Cross, *Phys. Rev. Lett.* 49, 1959 (1982).
105. J.P. Eisenstein and R.E. Packard, *Phys. Rev. Lett.* 49, 564 (1982).
106. Y. Sun, P. Wölfle, and S.K. Yip, *Phys. Rev. Lett.* 63, 1613 (1989).
107. R.C. Richardson, *J. Low Temp. Phys.*, 1076 (1980).
108. C.J. Pethick, H. Smith, and P. Bhattacharyya, *Phys. Rev. Lett.* 34, 643 (1975).
109. N.A. Greaves and A.J. Leggett, *J. Phys.* C16, 4383 (1983).
110. S. Yip and A.J. Leggett, *Phys. Rev. Lett.* 57, 345 (1986).
111. W.Z. Lin, R.W. Schoenlein, J.G. Fujimoto, and E.P. Ippen, *IEEE J. Quantum Electron.* 24, 267 (1988).
112. C.V. Shank, R.L. Fork, R.F. Leheny, and J. Shah, *Phys. Rev. Lett.* 42, 112 (1979).
113. C.V. Shank, R.L. Fork, R. Yen, J. Shah, B.I. Greene, A.C. Gossard, C. Weisbuch, *Solid State Commun.* 47, 981 (1983).
114. R.G. Ulbrich, J.A. Kash, and J.C. Tsang, *Phys. Rev. Lett.* 62, 949 (1989).
115. U. Rössler, *Solid State Commun.* 49, 943 (1984).
116. P.B. Allen, *Phys. Status Solidi (b)* 120, 529 (1983).
117. G. Fasol and H.P. Hughes, *Phys. Rev.* B33, 2953 (1986).
118. G. Fasol, K. Ploog, and E. Bauser, *Solid State Commun.* 54, 383 (1985).
119. D.N. Mirlin, I.Y. Karlik, and V.F. Sapega, *Solid State Commun.* 65, 171 (1988).
120. P. Wölfle, *Lectures on Solid State Physics II* (1987).
121. M. Liu, *Phys. Rev.* B18, 1165 (1978).
122. B. Castaing and P. Nozières, *J. Phys. (Paris)* 41, 701 (1980).
123. H. Wiechert and F.I. Buchholz, *J. Low Temp. Phys.* 39, 623 (1980).
124. H. Wiechert and F.I. Buchholz, *J. Low Temp. Phys.* 51, 291 (1983).
125. L.J. Buchholtz and G. Zwicknagl, *Phys. Rev.* B23, 5788 (1981).
126. L.J. Buchholtz, *Phys. Rev.* B33, 1579 (1986).

BIOGRAPHICAL SKETCH

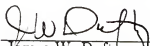
Yuanshan Sun was born on February 16, 1944 in Zhejiang, China. He was educated in several cities in China. He went to Nanjing University to study physics in 1963 and graduated in 1968. After three years of labour work at rural area, he was assigned to an electronic instruments manufactory as a technician. In 1979 he obtained an opportunity to take the entrance examination and became a graduate student of Nanjing University. He received his M.S. in 1982 and then joined the Low Temperature Physics Laboratory of Nanjing University as a teaching and research assistant. He came to the University of Florida in September 1985 to continue his graduate study for Ph.D. in physics. He began research under Professor Peter Wölffe in Fall 1986 and work on the theory of condensed matter physics.

I certify that I have read this study and that in my opinion it conforms to acceptable standards of scholarly presentation and is fully adequate, in scope and quality, as a dissertation for the degree of Doctor of Philosophy.



Peter K. Wölffe, Chairman
Professor of Physics

I certify that I have read this study and that in my opinion it conforms to acceptable standards of scholarly presentation and is fully adequate, in scope and quality, as a dissertation for the degree of Doctor of Philosophy.



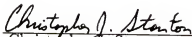
James W. Dufty
Professor of Physics

I certify that I have read this study and that in my opinion it conforms to acceptable standards of scholarly presentation and is fully adequate, in scope and quality, as a dissertation for the degree of Doctor of Philosophy.



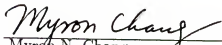
Neil S. Sullivan
Professor of Physics

I certify that I have read this study and that in my opinion it conforms to acceptable standards of scholarly presentation and is fully adequate, in scope and quality, as a dissertation for the degree of Doctor of Philosophy.



Christopher J. Stanton
Assistant Professor of Physics

I certify that I have read this study and that in my opinion it conforms to acceptable standards of scholarly presentation and is fully adequate, in scope and quality, as a dissertation for the degree of Doctor of Philosophy.



Myron N. Chang
Assistant Professor of Statistics

This dissertation was submitted to the Graduate Faculty of the Department of Physics in the College of Liberal Arts and Sciences and to the Graduate School and was accepted as partial fulfillment of the requirements for the degree of Doctor of Philosophy.

May 1990

Dean, Graduate School